Validation and Uncertainty Quantification of Doublet Lattice Flight Loads using Flight Test Data

Nicholai K. K. Olson

Thesis submitted to the Faculty of the

Virginia Polytechnic Institute and State University

in partial fulfillment of the requirements for the degree of

Master of Science

in

Aerospace Engineering

Mayuresh J. Patil, Chair

Rakesh K. Kapania

Christopher J. Roy

June 18, 2018

Blacksburg, Virginia

Keywords: Loads, Doublet Lattice, Validation, Uncertainty Quantification

Validation and Uncertainty Quantification of Doublet Lattice Flight Loads using Flight Test Data

Nicholai K. K. Olson

ABSTRACT

This paper presents a framework for tuning, validating, and quantifying uncertainties for flight loads. The flight loads are computed using a Nastran doublet lattice model and are validated using measured data from a flight loads survey for a Cessna Model 525B business jet equipped with Tamarack® Aerospace Group's active winglet modification, ATLAS® (Active Technology Load Alleviation System). ATLAS® allows for significant aerodynamic improvements to be realized by reducing loads to below the values of the original, unmodified airplane. Flight loads are measured using calibrated strain gages and are used to tune and validate a Nastran doublet-lattice flight loads model. Methods used to tune and validate the model include uncertainty quantification of the Nastran model form and lead to an uncertainty quantified model which can be used to estimate flight loads at any given flight condition within the operating envelope of the airplane. The methods presented herein improve the efficiency of the loads process and reduce conservatism in design loads through improved prediction techniques. Regression techniques and uncertainty quantification methods are presented to more accurately assess the complexities in comparing models to flight test results.

Validation and Uncertainty Quantification of Doublet Lattice Flight Loads using Flight Test Data

Nicholai K. K. Olson

GENERAL AUDIENCE ABSTRACT

This paper presents a process for correlating analytical airplane loads models to flight test data and validating the results. The flight loads are computed using Nastran, a structural modeling tool coupled with an aerodynamic loads solver. The flight loads models are correlated to flight test data and are validated using measured data from a flight loads survey for a Cessna Model 525B business jet equipped with Tamarack® Aerospace Group's active winglet modification, ATLAS® (Active Technology Load Alleviation System). ATLAS® allows for significant aerodynamic improvements and efficiency gains to be realized by reducing loads to below the values of the original, unmodified airplane. Flight loads are measured using a series of strain gage sensors mounted on the wing. These sensors are calibrated to measure aerodynamic loads and are used to tune and validate the Nastran flight loads model. Methods used to tune and validate the model include quantification of error and uncertainties in the model. These efforts lead to a substantially increased understanding of the model limitations and uncertainties, which is especially valuable at the corners of the operating envelope of the airplane. The methods presented herein improve the efficiency of the loads process and reduce conservatism in design loads through improved prediction techniques. The results provide a greater amount of guidance for decision making throughout

the design and certification of a load alleviation system and similar airplane aerodynamic improvements.

Acknowledgments

Thanks to my fellow engineers and mentors at Tamarack®, Nick Guida, Jacob Klinginsmith, and Dr. Michele Castellani, my advisor at Virginia Tech, Dr. Mayuresh Patil, and my wife and better half, Hailey, all to whom I am very grateful for the support they have given me over the past couple of years.

This work received support from Tamarack® Aerospace Group.

Contents

List of Figures

List of Abbreviations

α	angle of attack
β	angle of sideslip
M	Mach number
q	dynamic pressure
$KEAS$	knots equivalent airspeed
Nz	load factor in aircraft z-axis
δ_{TACS}	TACS (Tamarack® Active Camber Surface) deflection
$C_{L\alpha}$	doublet lattice strip lift curve slope
C_{Lo}	doublet lattice strip lift curve intercept
L	lift force
S_y	shear force along aircraft y-axis
S_z	shear force along aircraft z-axis
M_x	bending moment about aircraft x-axis
dM_x/dg	change in bending moment about aircraft x-axis with respect to change in aircraft g-loading
$\hat{y}_i$	Value of the dependent variable

$\hat{\sigma}^2$	Mean square error
$t_{\frac{\alpha}{2},n-(k+1)}$	One sided student t-value
x_i	Predictor variables
X	Matrix of values used to define the fit

Chapter 1

Introduction

Tamarack® Aerospace Group (Tamarack®) is the designer and manufacturer of ATLAS® (Active Technology Load Alleviation System), a patented [1] active winglet system installed on the Cessna Model 525B airplane (13870 lb gross takeoff weight). ATLAS® is the first load alleviation system of its type to be designed and certified for installation on FAA Part 23 [2] airplanes. The active winglet modification adds a wing extension with a load alleviation device (the TACS, Tamarack® Active Camber Surface) and a winglet to the existing wing, resulting in a significantly higher aspect ratio. Typically during winglet and wing extension modifications, wing loads are increased over the baseline aircraft creating a need for the wing to be strengthened. The TACS are designed to activate during high-g events and reduce wing loads at the design conditions, thereby reducing the additional load from the wing extension and winglet modification and negating the need for strengthening of the baseline wing. The net result is a system that allows for large performance improvements without the typical

structural detriments caused by typical winglet installations.

The development of such a system requires high fidelity and accurate loads models to be developed. Although Tamarack®'s ATLAS modification is a significant aerodynamic improvement to the airplane, it is a very simple installation. As a result, Tamarack® has the ability to perform a baseline flight test program and in a relatively short period thereafter perform an identical flight test program on the airplane equipped with the ATLAS® modification. The nature of this type of flight test program opens the door to many comparative techniques for loads substantiation, but the need for an absolute analysis persists. Often, in an effort to save time, extra layers of conservatism are added to models to ensure their validity throughout the application envelope of the model. Therefore, it is desirable from both a safety and cost standpoint to have an efficient process for computing the loads that leverages the ability to obtain rapid flight test results on both the baseline and modified aircraft.

The work performed in this document is an extension of the loads analysis and flight test performed for the certification of the ATLAS Modification for the Model 525B airplane. Flight test data and loads models were developed and tuned for certification, and are further explored in this document. The new methods presented herein improve the efficiency of the loads process and reduce conservatism in design loads through improved prediction techniques. New regression techniques and uncertainty quantification methods are presented to more accurately assess the complexities in comparing models to flight test results. The process used is a practical application of the verification and validation framework described

by Roy and Oberkampf [3].

This study will focus on the effects downstream of the flight test loads survey, as flight test loads calibration is a well developed and known problem, with the industry standard methods developed by NACA over 60 years ago [4]. In addition, some research has been performed more recently on the uncertainty quantification of these methods [5]. This study provides insights for relevant "Go/No Go" checks that can be performed to determine spurious flight loads data by assessing the model form of the data and provides several indicators of inaccuracies and errors.

This methodology contrasts to other studies published that develop methods to reduce computational burden in computing flight loads using surrogate models and uncertainty propagation methods such as Tartaruga et al [6], or others that look at structural or atmospheric uncertainties [7] [8]. This study focuses on using flight loads as the basis for a rapid and accurate flight loads assessment. Uncertainty quantification of the Nastran loads model is determined primarily using prediction intervals as was done by Hale et al [9] on aircraft stability parameters.

This document provides the process used for the validation and verification of the wing, winglet, and TACS load alleviation surface loads using flight test data. A good correlation of flight test data to the calculated loads has been achieved and the predictive capability of the model is determined. A complete flight loads survey has been performed that conforms to FAA Part 23 [2] regulations and uses methods prescribed by Lomax [10].

A summary of the contents of this paper is provided below.

- *Chapter 2 describes flight test maneuvers performed to measure loads data.* TACS sweep data were collected to determine a correction factor for the TACS surface. Wind-up turn and sideslip maneuver data were taken to tune and validate loads on the wing and winglet. These data were used throughout the process of tuning and validation.

- *Chapter 3 describes the Nastran model used for flight loads predictions.* Flight loads were calculated using Nastran, a general purpose finite element solver with capabilities for trimmed aeroelastic solutions.

- *Chapter 4 describes the tuning performed on the Nastran model to better match flight test data.* Nastran was tuned using Direct Matrix Input (DMI) commands to closely match flight test loads. Nastran cases were run through the loads solver at flight conditions matching the flight test points and the model was tuned to flight test spanwise bending moment distributions due to aerodynamic forces.

- *Chapter 5 validates and asseses uncertainties and predictive capability of model.* Validation and uncertainty quantification of the tuned Nastran loads model was performed using several methods. The prediction intervals of model form uncertainty were computed and techniques are provided for assessing the model accuracy throughout the flight envelope. A Multiple Linear Regression (MLR) model was developed and discussed to aid in the effort. The model is validated by comparing loads outputs of the final tuned model at matching flight conditions to flight test points.

Chapter 2

Flight Testing

A complete flight test loads survey was conducted for the tuning and validation effort. A comprehensive data acquisition system was installed to measure flight conditions and aircraft parameters in real-time throughout the flight. The wing and winglet were instrumented with a series of strain gages and were calibrated on the ground for both strain and moment using industry accepted methods [4]. Loads data were measured in terms of "net loads", the absolute load applied to the wing in a given maneuver, which is the sum of inertial and aerodynamic loads. The data were further reduced using known mass distributions to isolate aerodynamic loads for this study. Throughout this document, all loads data are presented in terms of aerodynamic loading only unless explicitly stated otherwise.

Multiple datasets were collected throughout the flight test program. This document does not explicitly state the number of datasets used to tune and validate the model, but does

give guidance on how to give relevant and statistically reliable results. The majority of the datasets collected were used for tuning the Nastran models and developing Multiple Linear Regression (MLR) models, and some of the datasets were used for validation. Sample sizes used in all statistical analyses were determined based on the number of maneuvers performed. In other words, a given wind-up turn was assumed to be one sample, as opposed to the thousands of data points measured during that maneuver, conservatively increasing the uncertainty bounds. This technique has been chosen because boundary conditions change slightly between different types of maneuvers, not every flight had identical aircraft configurations, and every flight is prone to slightly varying environmental conditions, which are not accounted for in this study.

A basic assumption made for the purpose of this study is that the measured flight test loads are assumed to be accurate, and the uncertainties in the flight load measurements process are not assessed. This study instead assesses the predictive capability of the flight test loads model as shown in subsequent sections. When performing a flight loads survey, often only a small portion of the aircraft operating and loads envelope can be assessed. The image below shows three envelopes. The gust and maneuver envelopes define the operating envelope of the airplane for a given aircraft weight and altitude. The validation envelope is overlaid and shows where flight testing was conducted and used to quantify the predictive capability of the model. Note that the gust and maneuvering envelopes for an altitude of 20,000 ft and at the maximum zero fuel weight are shown because this represents the flight condition where many of the critical loads cases occur. Load cases tend to be most critical at these flight

conditions because of a critical combination of high gust load factors, small Mach effects, and a lack of inertial relief from fuel in the wings.

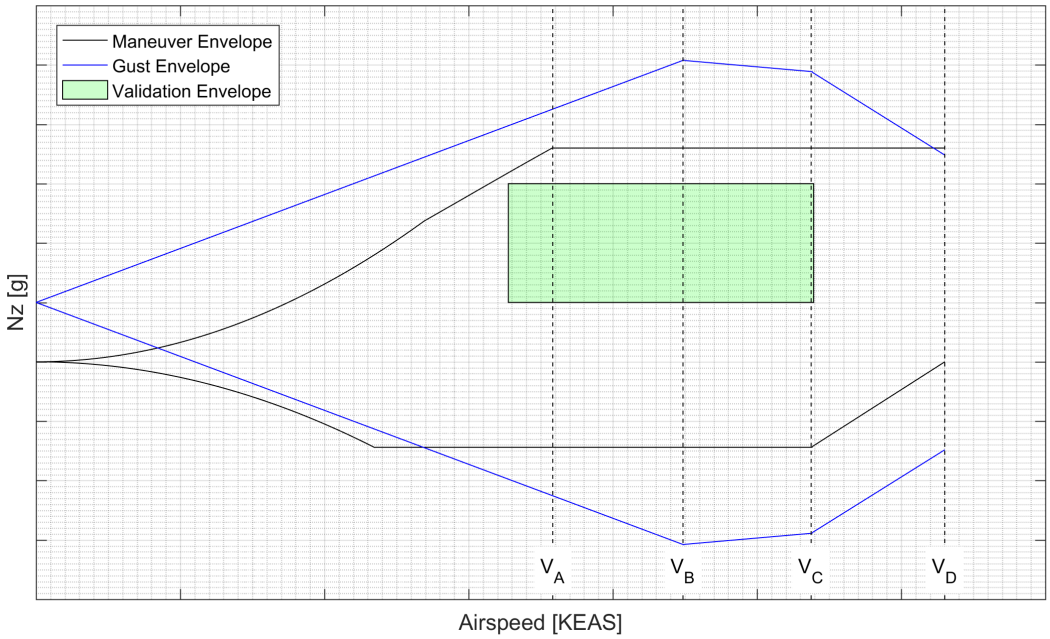

Figure 2.1: Model 525B Airplane V-n Diagram, Max Zero Fuel Weight, 20,000 ft.

Fig. 2.1 shows that the requirement for loads prediction of the gust and maneuver envelopes extend well outside of the validation envelope, where it is both impractical and unsafe to perform flight testing. This is the primary area of concern for the study presented herein. Flight testing is only performed within the validation envelope for three primary reasons. Flight testing is performed below the critical airplane load factors to provide adequate safety margins for crew and airplane structural integrity. Flight testing is performed below the maximum airspeed and altitude/Mach limits to reduce dynamic instabilities inherent to flight in these regimes. Finally, all flight testing is performed at positive load factors only due to the impracticality of flight at negative load factors and potential damage to aircraft

engines and systems.

All flight test loads are "trimmed maneuvers", meaning that the flight test pilot is balancing all input forces with the necessary control inputs to keep the airplane as close as possible to a trimmed flight state. This is one of the primary reasons all flight test maneuvers are performed at low altitudes and Mach numbers, as dynamic instabilities can be minimized. However, even with an experienced flight test pilot, the more dynamic the condition, the more likely for noise to occur in a given maneuver. With sufficient datasets, this noise can be minimized and effectively filtered. Efforts to match these balanced conditions are accounted for in the Nastran loads solution using the "TRIM" card, but can never truly be assessed without measuring and quantifying the loads on every surface. For the purpose of this study, allowing Nastran to trim the airplane using relevant control surfaces is assumed to be sufficient, and the trim control surface uncertainties are not included in the model form. This is a simplifying assumption that adds uncertainty to the models, but will be captured in the uncertainty analysis. Each type of maneuver has slightly different boundary conditions, and thereby will have differing mean values, increasing model form uncertainty.

Three types of flight test maneuvers are used in the tuning and validation process; wind-up turn maneuvers for the wing, sideslip maneuvers for the winglet, and sweeps of the TACS for surface load influences. Each of these maneuvers were chosen to isolate the loads for different lifting surfaces and are a standard set of maneuvers for loads flight testing [11], with the exception of the TACS sweeps, which are specific only to an airplane equipped with the ATLAS load alleviation system.

2.1 Wind-up Turn Maneuvers

A wind-up turn is a maneuver where the airplane enters into a banked turn and slowly decreases the radius of the turn while maintaining the airspeed of the airplane, thus increasing the aircraft load factor throughout the maneuver. Wind-up turn maneuvers are balanced primarily by a significant elevator input, but also by aileron and rudder inputs to maintain the necessary turning attitude. Performing maneuvers in both directions back to back is an effective method for reducing bias from aileron and rudder inputs, since these inputs are not included in the model form. Data are extracted from the increasing load factor portion of the wind-up turn where the data are the cleanest and most controlled before turning out of the maneuver. A plot of wind-up turn maneuver data is shown in Fig. 2.2.

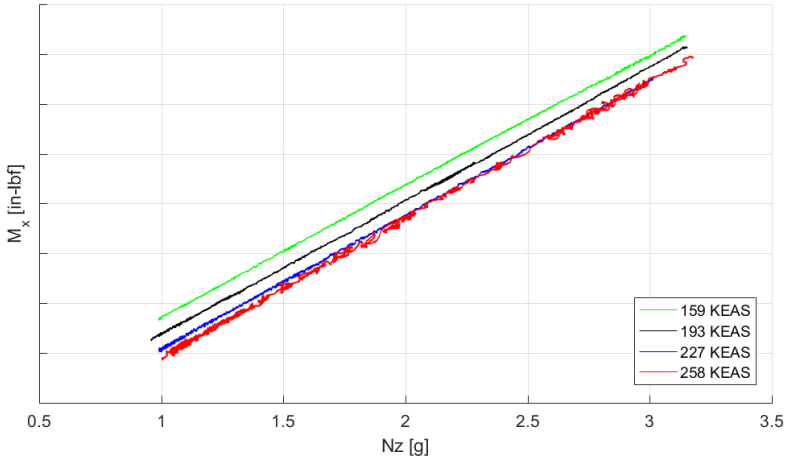

Figure 2.2: Wind-up turn maneuver flight test loads.

2.2 Sideslip Maneuvers

A sideslip is a maneuver performed by introducing a rudder input to yaw the airplane. Because winglets are a nearly vertical surface, sideslip maneuvers have a much more significant impact on the effective angle of attack on the winglet surface and are very valuable in quantifying the lift-curve of the winglets. Sideslip maneuvers are balanced by aileron inputs to maintain a straight flight path and level 1g flight attitude. A plot of winglet bending moments with respect to β for the entire sideslip maneuver is shown in Fig. 2.3. For tuning and validation, winglet data were only extracted between +/- 8 degrees of sideslip because the winglet stalls above this angle. Data are also only taken in the direction of increasing sideslip angle, as the condition becomes much more dynamic when releasing rudder inputs.

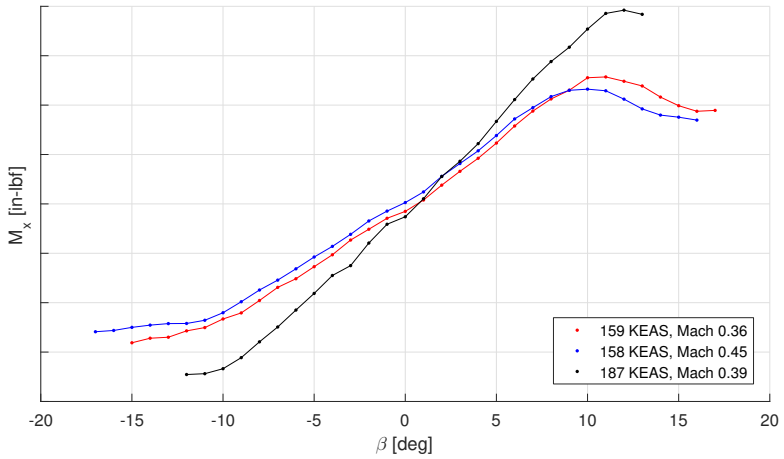

Figure 2.3: Sideslip maneuver flight test winglet loads.

2.3 TACS Sweeps

A TACS sweep maneuver is a simple maneuver where TACS load alleviation surfaces are brought under manual control and swept through their entire range of motion while the airplane flies straight and level at 1g. Only elevator inputs are required to balance small changes in spanwise lift and pitching moment from the change in TACS deflection (δ_{TACS}). Fig. 2.4 shows the response in wing bending moment during the TACS sweep maneuvers.

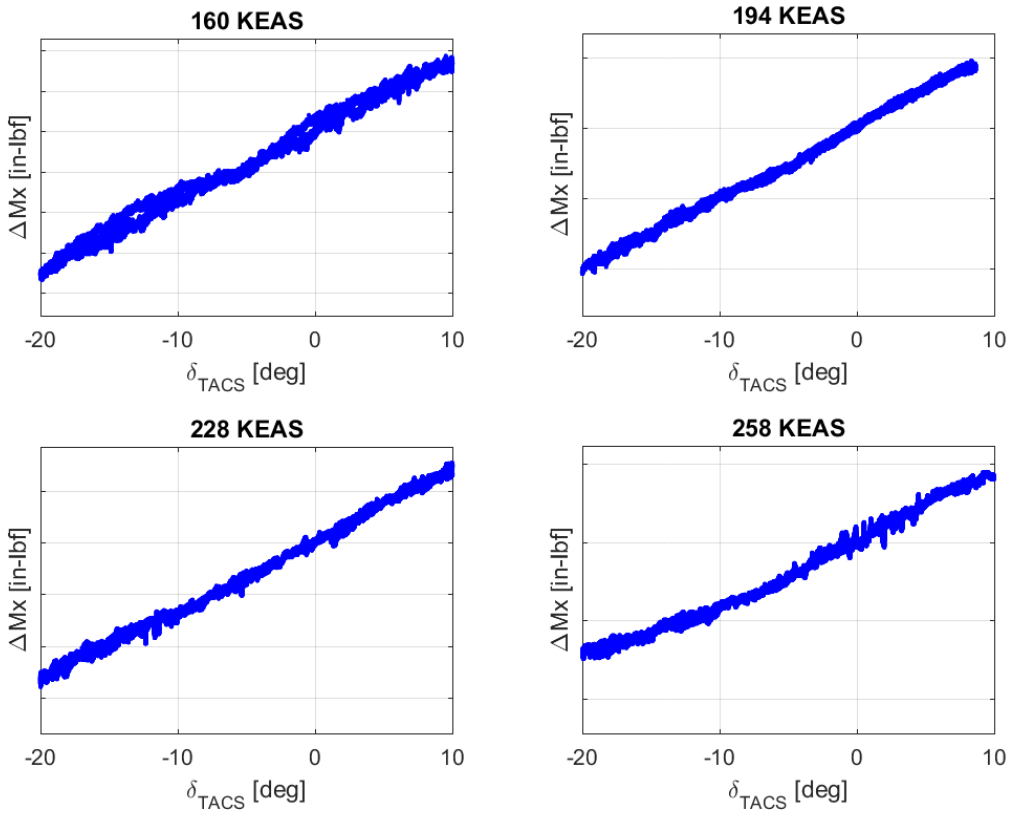

Figure 2.4: TACS sweep maneuver flight test loads.

Chapter 3

Nastran Model

The loads calcuations are carried out using Nastran, a general purpose finite element solver which includes solutions for aeroelastic analysis. The aeroelastic model is generated by coupling a finite element structural model with a doublet lattice aerodynamic model. A static aeroelastic trim is computed using the Nastran Static Aeroelasticity Solution (SOL 144). The corrections made to the Nastran model in this study are computed in terms of SOL 144, where the aerodynamic forces are balanced with either aircraft inertial characteristics or control surface deflections. Throughout the certification process of the Model 525B, other Nastran aeroelasticity solutions are utilized as well, including the Aerodynamic Solution (SOL 145) and the Dynamic Aeroelastic Response Solution (SOL 146). These solutions benefit from aerodynamic correction factors[12] as well, increasing the need for tuning of the Nastran aeroelastic model.

The aerodynamic model is generated using a doublet lattice method which solves the linearized potential flow equations (including a correction for compressibility). The aerodynamics used in this analysis are modeled using flat panels to represent all major branches of the aircraft. Each lifting surface is divided into spanwise "strips" and further into chordwise elements, known as "boxes." The potential flow solution integrates the lift on the airplane as a whole, and as a result considers interference effects between all boxes. The trailing vortices assure that downwash of leading panels is included in those panels downstream (i.e., downwash from the wing onto the tail surfaces is implicit in the solution)[13]. Fig. 3.1 shows the aerodynamic boxes on the right wing of the loads model.

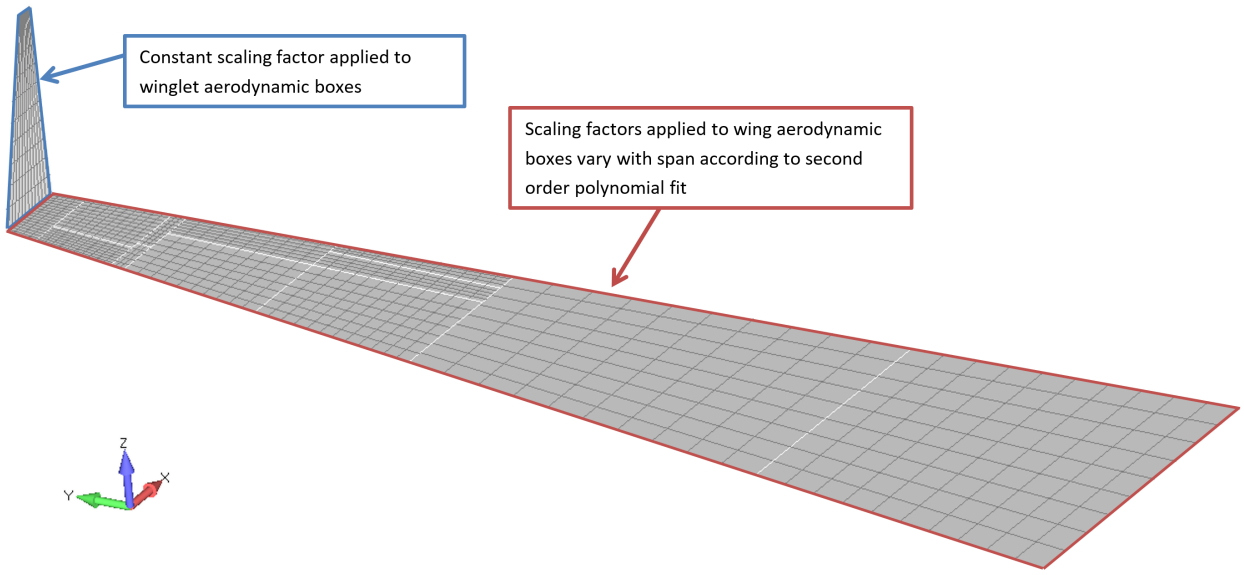

Figure 3.1: Wing aerodynamic boxes.

The aerodynamic and structural grids are connected via interpolation such that any aerodynamic and inertial forces that are introduced into the structural model and structural deflections are likewise introduced into the aerodynamics. The resulting aerodynamic load-

ing includes the effect of the deformation of the flexible aircraft model.

The doublet lattice method has the benefit of solving loads quickly without the need for a more computationally expensive Navier-Stokes solution. However, because it is a potential flow solution it does not consider viscous effects or other flow nonlinearities, and it often over-predicts the lift-curve of lifting surfaces by 20-30%. Furthermore, simplified models do not include all geometric aircraft features which inherently produce solutions that are not truly representative of reality. As a result, it is often necessary to introduce corrections and limitations in the solution or in pre/post-processing. Nastran includes provisions for correcting the lift-curve slope of lifting surfaces by factoring the effectiveness of each aerodynamic box. These provisions are discussed in further detail in Chapter 4.

For the purpose of the Model 525B loads survey, several characteristics are captured via pre-processing of the loads and experimental corrections. First, trailing edge device nonlinearities occur in the TACS due to geometric changes that are not effectively captured in the doublet lattice solution. Because of this, a TACS correction factor is computed to be applied in pre-processing to account for local nonlinearities of the deflected surface. Additionally, the complete lift distribution on the wing and winglet is compared to experimental data and correction factors are computed to help the lift distribution better match reality. Scaling factors can be developed for one or many flight conditions as necessary.

Transonic effects on the model as a whole are not considered in the corrections. The Model 525B is capable of flying in the low transonic range, but critical cases generally do not occur in this region. Furthermore, the doublet-lattice implementation used by Nastran does a

reasonable job predicting mach effects[12][14]. For completeness Mach is considered in the validation and uncertainty quantification as described in Chapter 5, but its effects are shown to be small.

The untuned Nastran loads model includes no $C_{L\alpha}$ scaling and C_{Lo} scaling only in the form of the W2GJ matrix, which uses wing twist and camber geometry but no flight test data. The tuned Nastran model computes new C_{Lo} scaling in the form of the FA2J matrix and $C_{L\alpha}$ scaling in the form of a WKK matrix, which is a premultiplication scaling factor matrix originally suggested by Giesing, Kalman, and Rodden [15]. The scaling varies spanwise, but is constant in the chordwise direction as Nastran does a reasonable job of predicting chordwise distributions on lifting surfaces. Only one set of scaling factors is computed for all flight conditions, as it shows a good match throughout the validation envelope of the Model 525B airplane. The tuning process and results are described in Chapter 4.

Chapter 4

Model Tuning

The purpose of this section is to describe how tuning of the Nastran loads model was performed in order to better match flight test results. The tuning described herein uses flight test loads data to find correction factors for the δ_{TACS} effectiveness and derive scaling factors for $C_{L\alpha}$ and C_{Lo} of aerodynamic boxes of the wing and winglet lifting surfaces. These tuning corrections are a high level implementation of common techniques used to update the Nastran Aerodynamic Influence Coefficient (AIC) matrices from Computational Fluid Dynamics (CFD) data [16][17][18]. δ_{TACS} correction factors were developed as a pre-processing procedure before running the Nastran model. Aerodynamic box tuning was performed by comparing flight test bending moments to the untuned Nastran model. These comparisons allowed for scaling of Nastran lift curves to develop loads that are a better representation of flight test loads. Nastran Direct Matrix Input (DMI) commands were used to input a scaling factor for both $C_{L\alpha}$ and C_{Lo} to the aerodynamic boxes.

4.1 TACS Efficiency Correction

In this section, a correction factor is derived to correct the TACS deflections (δ_{TACS}) for the nonlinear characteristics that occur with dynamic pressure and surface deflections. The result of the correction is an efficiency factor, called $\eta_{\delta_{TACS}}$, that is multiplied by the TACS deflection in pre-processing, providing a scaled TACS deflection as the input to the Nastran loads model. This methodology maps the "effective deflection" of the TACS to the "geometric deflection," taking into account any nonlinearities that occur with increasing q and varying δ_{TACS}.

A multiple linear regression model (MLR) is first developed to represent flight test data across the range of q and TACS deflections. The order of each variable within the MLR was determined using first principles and trial and error. The resulting representation of the MLR is presented below.

$$\Delta M_{x_{FT}}(q, \delta_{TACS}) = B_0 + B_1 qM + B_2 q\delta_{TACS} + B_3 q\delta_{TACS}^2 + B_4 q\delta_{TACS}^3 \tag{4.1}$$

The quantity of interest is an incremental bending moment on the wing ($\Delta M_{x_{FT}}$) as control surface inputs are typically quantified as an incremental loads input. The MLR is developed from flight test bending moments measured during TACS sweeps maneuvers. To find $\Delta M_{x_{FT}}$, the TACS deflected bending moments must be subtracted from the trimmed 1g bending moments to isolate the effects of the TACS. Using the MLR, the loads are offset so they have a zero y-intercept.

$$\Delta M_{x_{FT}}(q, \delta_{TACS}) = M_{x_{FT}}(q, \delta_{TACS}) - M_{x_{FT}}(q, \delta_{TACS} = 0) \tag{4.2}$$

To perform the comparisons between Nastran and the flight test data, unit TACS deflection cases were run in Nastran with same flight conditions as the flight test loads. Based on the assumption of linear aerodynamics of the potential flow solution and the consistency between each TACS sweep flight test point, only four unit cases were computed. The loads were then interpolated to get the correct value of q for a given δ_{TACS}. The aerodynamic M_x was then extracted for each Nastran loads case.

Using the Nastran unit radian case, a least squares fit was applied to match the Nastran loads to the flight test loads. The resulting scaling factor (SF) of this case is the necessary TACS deflection needed to meet the moment due to flight test TACS deflections.

$$min(R^2(SF)) = min\Big(\sum \left[\Delta M_{x_{FT}}(q, \delta_{TACS}) - \Delta M_{x_{NAS}}(q, \delta_{TACS_{NAS}} = 1 \text{ rad}) \times SF\right]^2\Big) \tag{4.3}$$

The final step is to divide TACS required by geometric δ_{TACS} to compute $\eta_{\delta_{TACS}}$.

$$\eta_{\delta_{TACS}} = \frac{\delta_{TACS_{NAS}} \times SF}{\delta_{TACS}} \tag{4.4}$$

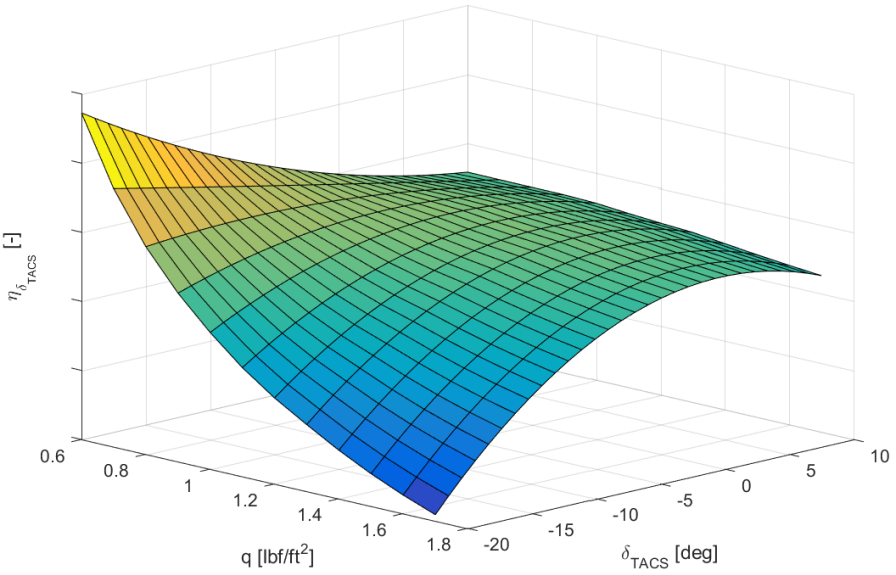

Figure 4.1: TACS efficiency correction factors.

4.2 Wing and Winglet Tuning Results

The purpose of this section is to describe the Nastran loads model wing and winglet tuning procedures and results. The model lifting surfaces were tuned for both C_{Lo} and $C_{L\alpha}$ by scaling all aerodynamic boxes by scaling factors using the functionality of Nastran Direct Matrix Input (DMI) commands.

A summary of the different DMI matrices used to tune the model are provided below [13].

- **W2GJ:** The W2GJ matrix is known as the Static Aerodynamic Downwash matrix and provides an offset to the doublet lattice downwash matrix. The W2GJ matrix is a vector that contains an input angle (radians) for each aerodynamic box. This can be used to tune the C_{Lo} of the aerodynamic boxes for downwash offsets that may arise due to camber and twist. For the Model 525B, the W2GJ matrix was computed from the wing geometric camber and twist and was used in the untuned Nastran loads model to generate $\alpha = 0$ degree pressure coefficients on the aerodynamic boxes to be scaled in the FA2J matrix. Also, it is important to note that the WKK matrix affects the entire downwash term, scaling both the C_{Lo} and $C_{L\alpha}$ terms, and therefore should be considered when computing the W2GJ matrix.

- **FA2J:** The FA2J matrix is very similar to the W2GJ matrix, except that it provides pressure coefficients that provide an offset to the total pressure coefficient computed on each aerodynamic box. The FA2J is a vector that contains an input coefficient of pressure (dimensionless) for each aerodynamic box. Like the W2GJ, this can be used

to tune the C_{Lo} of the aerodynamic boxes for downwash offsets that may arise due to camber and twist. For the Model 525B, the FA2J is computed by scaling the untuned $\alpha = 0$ degree pressure coefficients on the aerodynamic boxes to match flight test data.

- **WKK:** The WKK matrix is a matrix of correction factors used to scale each aerodynamic box lift curve slope. This can be used to tune the $C_{L\alpha}$ on each aerodynamic box to agree with flight test data. The WKK is a square matrix containing one scaling factor (dimensionless scalar value) for each aerodynamic box lift and moment in the diagonal. The off diagonal terms of the WKK matrix contain scaling factors for aerodynamic box influences on one another, but were left unchanged as they provide little value for the scope of this project. For the Model 525B, the WKK matrix was computed by comparing bending moment due to aerodynamic forces on the wing and winglet to the flight test values.

Aerodynamic box tuning is perfomed with respect to an effective angle of attack (α_{eff}) on each aerodynamic box. This allows wing and winglet tuning to be grouped into a single optimization routine. α_{eff} is a function of α, β, and the wing dihedral, (Γ). The equation to compute α_{eff} is shown below.

$$\alpha_{eff} = \alpha \cos(\Gamma) + \beta \sin(\Gamma) \tag{4.5}$$

This methodology provides a single parameter that can be used to relate the direction of the freestream flow to the orientation of an aerodynamic box at an arbitrary position and angle on the wing.

A total of 38 specific flight test points were extracted for tuning. Each of these cases were selected to envelope the entire range of flight test wind-up turn maneuver and slideslip maneuver flight conditions. The data were extracted by averaging all points within a small tolerance of a nominal Nz for wind-up turn maneuvers, and likewise within a small tolerance of a nominal β for sideslip maneuvers. Flight test data were post-processed to remove inertial loads from the measured net loads, resulting in an aerodynamic bending moment distribution. The aerodynamic bending moments were used in the comparisons to the Nastran loads.

Subsequently, Nastran cases were run with identical flight conditions to the 38 flight test points. Lift on each aerodynamic box, L_{box} was extracted for the flight test points. Using the lift on each aerodynamic box, and flight test points for the same wind-up or sideslip maneuver (where the flight conditions q, M, d_{TACS}, are virually constant), Nastran $C_{L_{\alpha_{eff}}}$ and C_{L_0} for each aerodynamic box can be derived. These parameters are required for the Nastran aerodynamic scaling DMI matrices. The equation used for deriving these values is shown below for reference.

$$L_{box} = qS\big(C_{L_{\alpha_{eff}}}\alpha_{eff} + C_{L_0}\big) \tag{4.6}$$

Once the $C_{L_{\alpha_{eff}}}$ and C_{L_0} terms were found, Eq. 4.6 can be modified to include the relevant scaling factors; the WKK scaling for the lift-curve slope (WKK_{box}), and the FA2J for the zero-lift offset ($FA2J_{box}$).

$$L_{box_{scaled}} = qS\big(WKK_{box}C_{L_{\alpha_{eff}}}\alpha_{eff} + FA2J_{box}C_{L_0}\big) \tag{4.7}$$

The lift on each aerodynamic strip, L_{strip}, was computed by summing lift on each aero-

dynamic box at constant chordlines. Using the lift on each strip, M_x on the wing was computed using a "forward rectangular rule," where the outboard shear is first derived by summing the spanwise lift, then the shear is multiplied by the distance between centroids of the aerodynamic strip of interest and the outboard aerodynamic strip to compute the moment increment. Summing this moment increment with the outboard moment provides the moment at the strip of interest. This method is selected because it is consistent with Nastran's methods used for the computation of beam moments, which are the final moments extracted for net loads outputs. Because this is a numeric procedure that differs from the common trapezoidal rule, the derivation is provided explicitly below.

$$S_y = \sum_{i=n}^{n_{tip}} -L_{strip_i} sin(\Gamma_i) \tag{4.8}$$

$$S_z = \sum_{i=n}^{n_{tip}} L_{strip_i} cos(\Gamma_i) \tag{4.9}$$

$$M_{x_{NAS}} = \sum_{i=n}^{n_{tip}} -S_{y_i} d_{z_i} + \sum_{i=n}^{n_{tip}} S_{z_i} d_{y_i} \tag{4.10}$$

For Eq. 4.8 - Eq. 4.10 d_{y_i} and d_{z_i} are the distance between the centroid of the aerodynamic strips at indices n and $n+1$. The WKK_{box} and the $FA2J_{box}$ parameters are computed using a simple optimization. The optimization is designed to minimize the true percent relative error, ϵ_t, between the Nastran and flight test aerodynamic M_x loads for all flight test conditions considered. This is shown below in Eq. 4.11.

$$min(\epsilon_t) = min\left(\sum_{i=1}^{n_{FTPoint}} \frac{|M_{x_{FT_i}} - M_{x_{NAS_{scaled\,i}}}|}{|M_{x_{FT_i}}|} \right) \tag{4.11}$$

Both WKK_{box} and the $FA2J_{box}$ are scaled using a second order polynomial along the main

portion of the wing. This scaling factor varies with the wingspan and is represented below for reference.

$$WKK_{box_{wing}} = C_{2_{WKK}} y^2 + C_{1_{WKK}} y + C_{0_{WKK}} \tag{4.12}$$

$$FA2J_{box_{wing}} = C_{2_{FA2J}} y^2 + C_{1_{FA2J}} y + C_{0_{FA2J}} \tag{4.13}$$

WKK_{box} and the $FA2J_{box}$ are scaled using constant factors for the entire winglet surface, $C_{winglet_{WKK}}$ and $C_{winglet_{FA2J}}$, respectively. In total, the optimization function includes a total of eight independent variables, $C_{0_{WKK}}$, $C_{1_{WKK}}$, $C_{2_{WKK}}$, $C_{winglet_{WKK}}$, $C_{0_{FA2J}}$, $C_{1_{FA2J}}$, $C_{2_{FA2J}}$, and $C_{winglet_{FA2J}}$, which are used to minimize the true percent relative error between $M_{x_{FT}}$ and $M_{x_{NAS_{scaled}}}$, as shown in Eq. 4.11.

The resulting scaling factors developed along the length of the span are shown below with respect to the normalized wingspan, η, of the Model 525B airplane including the ATLAS modification.

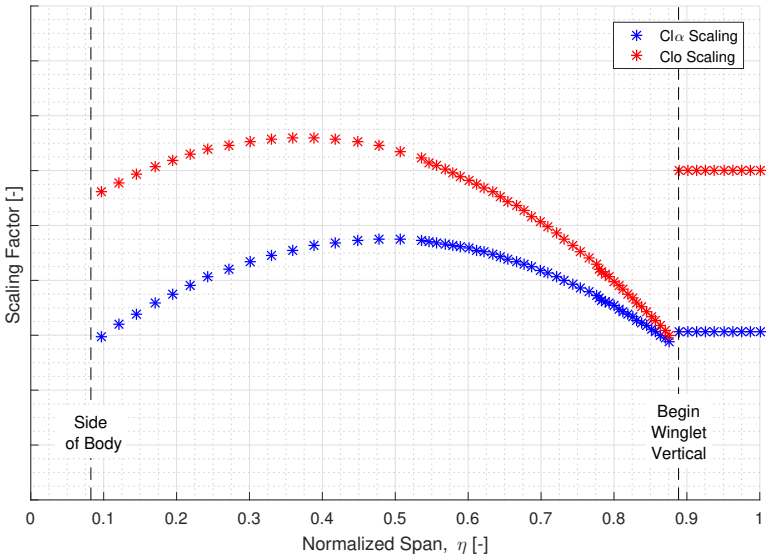

Figure 4.2: WKK and FA2J Scaling Factors.

The following plots are provided to show the effect of tuning on the moment response with respect to load factor (Nz) and spanwise moment distributions for a low speed, high angle of attack wind-up turn maneuver with the TACS in the neutral position ($\delta_{TACS} = 0$ deg). In the left hand plot, the bending moment for an inboard wing section is plotted for the untuned and tuned Nastran models versus the flight test results. Fig. 4.3 shows that a significant amount of error in both the slope and offset of the moment curve was present before tuning, but is greatly improved after tuning. The right hand plot shows the families of spanwise moment distributions data points extracted at 1g and 2g. The untuned model shows a generally good match at low load factors, but an increasing deviation at high load factors. The tuned model shows a much better match to flight test for all conditions.

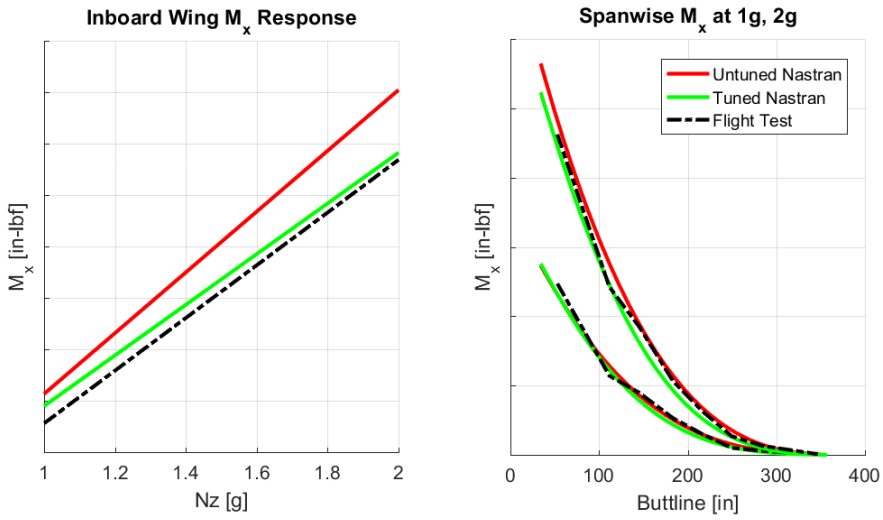

Figure 4.3: Tuning results for low speed wind-up turn maneuver with $\boldsymbol{\delta_{TACS} = 0}$ deg

Fig. 4.4 shows the same data for a high speed case with the TACS deflected upward to -20 degrees. Nastran is a poor predictor of trailing edge device loads, which can clearly be seen in the untuned model. The tuned model shows a much better fit of the moment response with respect to Nz as well as the spanwise distributions.

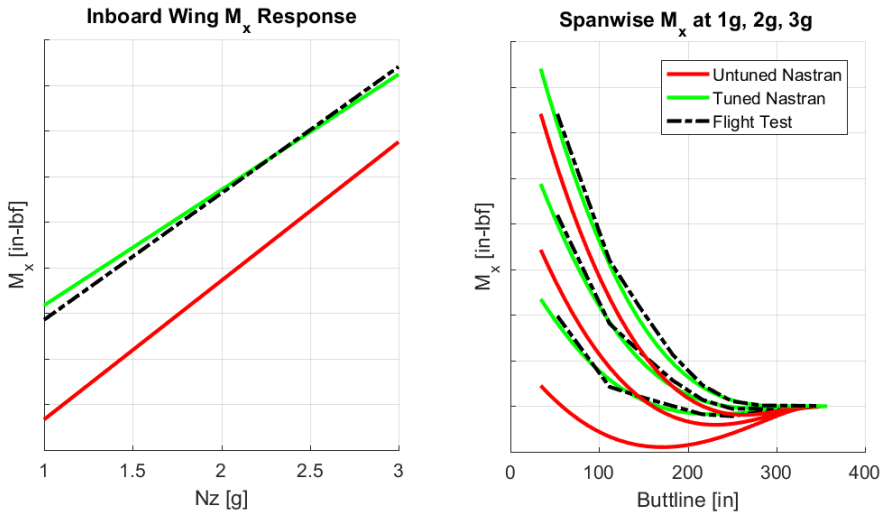

Figure 4.4: Tuning results for high speed wind-up turn maneuver with $\boldsymbol{\delta_{TACS} = -20}$ deg

Fig. 4.5 shows a comparison of the moment response with respect to sideslip angle, β, of the winglet surface. As with the two previous examples, this plot shows a mismatch in the untuned model, with the tuned model improving the fit significantly.

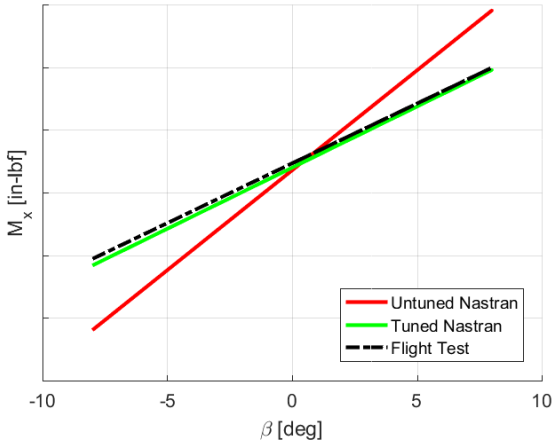

Figure 4.5: Winglet tuning results for sideslip maneuver.

Chapter 5

Nastran Model Validation and Uncertainty Quantification

This section describes the validation and uncertainty quantification of the Nastran loads model with experimental flight test data. Several methods are explored to best quantify the uncertainties and improve the model predictions. For all validation techniques, the tuning, validation, and model form uncertainty quantification of the Nastran Model developed herein would be referred to as "intrusive" methods [19], as the wing planform distribution is updated to better match the experimental data before performing an uncertainty quantification, as shown in Chapter 4. Separate datasets are used for tuning and validation to ensure that model updating provides results that are repeatable and reliable. The parameter we are most interested in quantifying and validating is the estimated model form uncertainty between the flight test loads data and the Nastran loads data.

Three different validation techniques are provided in this chapter. The first, presented in Chapter 5.1, follows traditional techniques used in industry of showing accurate flight test data, then validating the model within the validation envelope. This technique is presented to give a baseline for the subsequent strategies. The second technique, presented in Chapter 5.2, uses prediction intervals to quantify uncertainties of the Nastran model and extend those uncertainties to the critical flight test data points along the boundaries of the operational envelope. Finally, a method using a Multiple Linear Regression model (MLR) to quantify the error of the Nastran model is developed. The final method is the most accurate comparison between the Nastran data and the flight test loads and is presented in Chapter 5.3.

For validation, the Nastran loads set was expanded to include several hundred cases with flight conditions covering the entire experimental flight test envelope. A 5D linear interpolation on each of the independent variables (Nz, M, q, δ_{TACS}, and β) was performed to be able to compare Nastran loads to flight test loads at the same flight conditions as each individual flight test data point. The selection of these independent variables follows the methodology of matching the type of flight test maneuver with Nastran balanced maneuver conditions discussed in Chapter 2. Using the Nastran values interpolated to the same flight conditions as each flight test point, flight test and Nastran were simply subtracted to find the difference for each flight test data point.

Throughout this chapter loads plots, uncertainty quantification, and validation plots are presented to qualitatively show the results. These plots are provided for three different locations along the wing: at a location on the inboard third of horizontal portion of the

wing, a location on the outboard third of the horizontal portion of the wing, and at a location on the winglet. In each of the different validation and uncertainty quantification techniques, comparisons are made between flight test and Nastran loads. For reference, a comparison of flight test and Nastran loads is provided below to show relative magnitudes of the two datasets. Fig. 5.1, Fig. 5.2, and Fig. 5.3 provide comparisons for the inboard wing, the outboard wing, and the winglet, respectively.

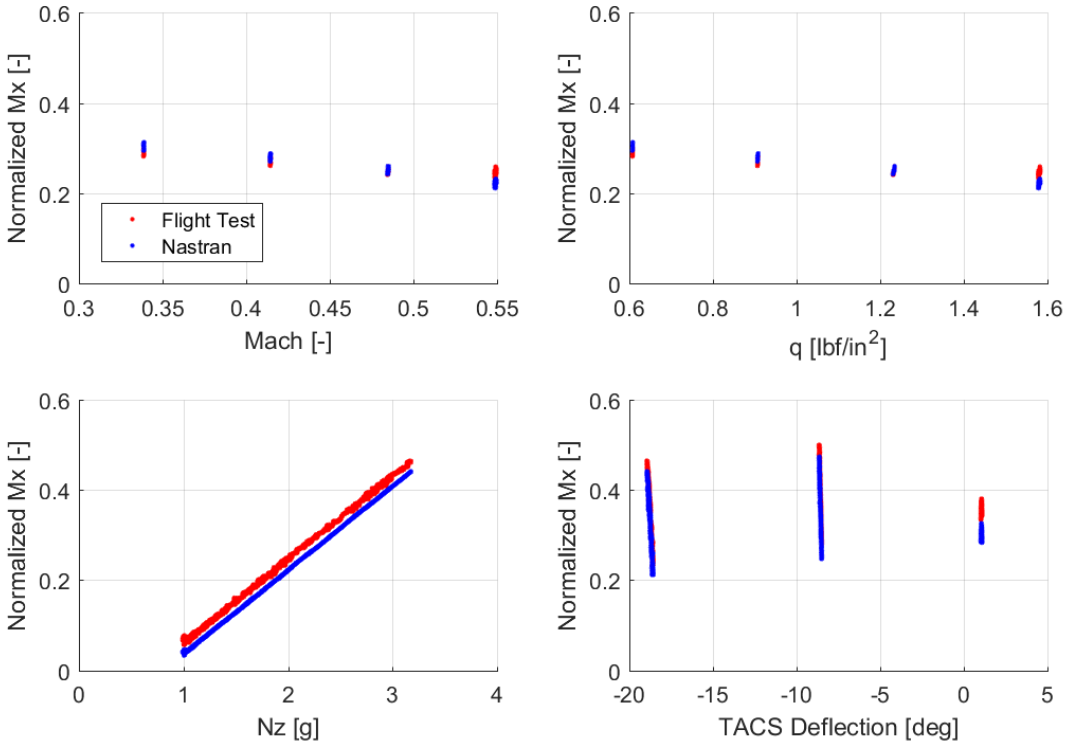

Figure 5.1: Inboard Wing flight test and Nastran M_x

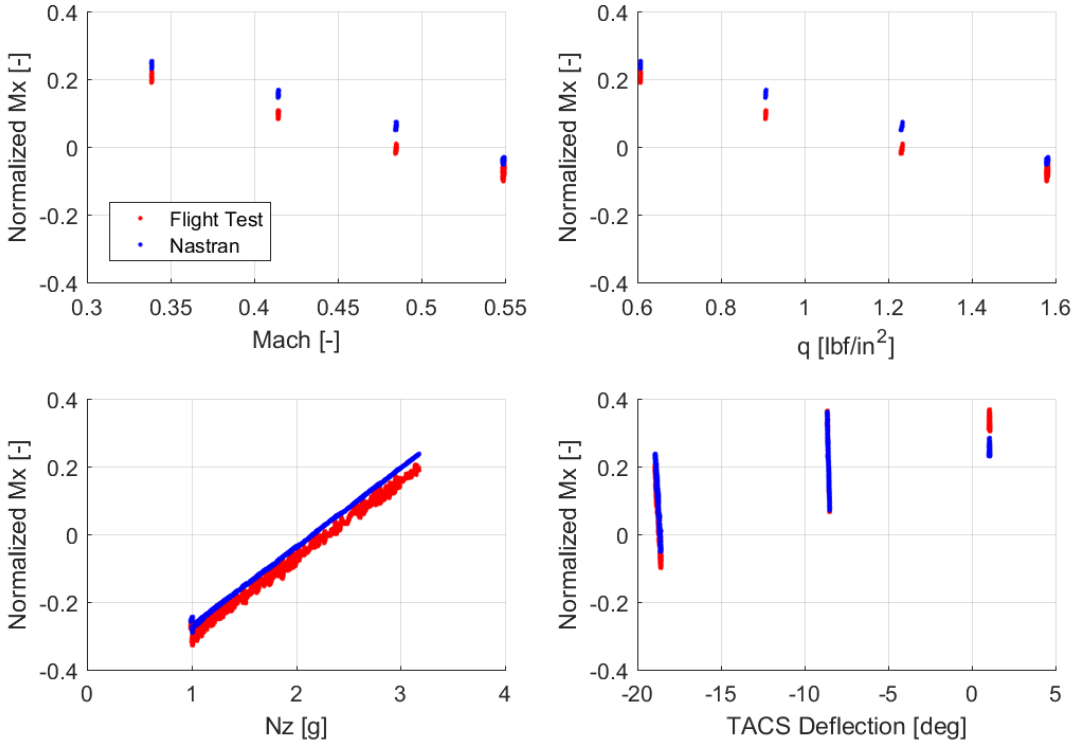

Figure 5.2: Outboard Wing flight test and Nastran M_x

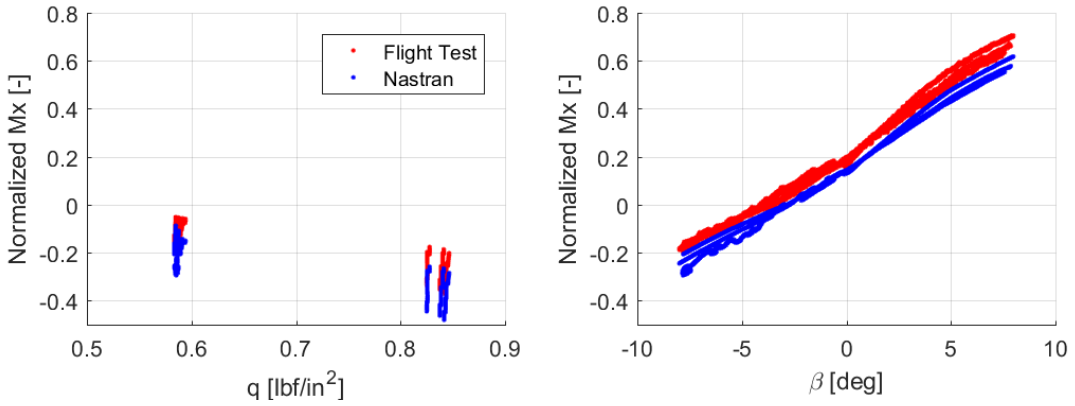

Figure 5.3: Winglet flight test and Nastran M_x

Several different techniques will be provided for presenting the estimated model form uncer-

tainties throughout this section. Results are presented qualitatively using a variety of plots, primarily relying on loads normalized to the maximum positive limit load for each location on the wing presented.

Estimated model form uncertainties and error are plotted against flight test data and the operational envelope in a variety of contexts to give insight to the model accuracy and uncertainty the at critical flight conditions. These various plots will be explained further in the context of the relevant plot. V-Mx diagrams, a variation of the common V-n diagram shown in Chapter 2, are used to show normalized gust and maneuver loads at a particular wing station across the operational loads envelope. This plot allows for the estimated model form uncertainties and error to easily be overlaid in a manner familiar to loads engineers to show the model accuracy and how it differs based on the changing flight conditions across the operational envelope. V-Mx diagrams showing only the Nastran model predictions for inboard and outboard sections of the horizontal portion of the wing are provided in Fig. 5.4, Fig. 5.5. The plots compute loads for vertical gusts and steady pitching maneuvers on the aircraft, and dominate loads on the horizontal portion of the wing. V-Mx diagrams for the winglet are provided in Fig. 5.6 and subsequent winglet V-Mx plots display sideslip maneuver loads, as winglet loads have been found to be dominated by overshoot maneuvers and the winglet stall angle.

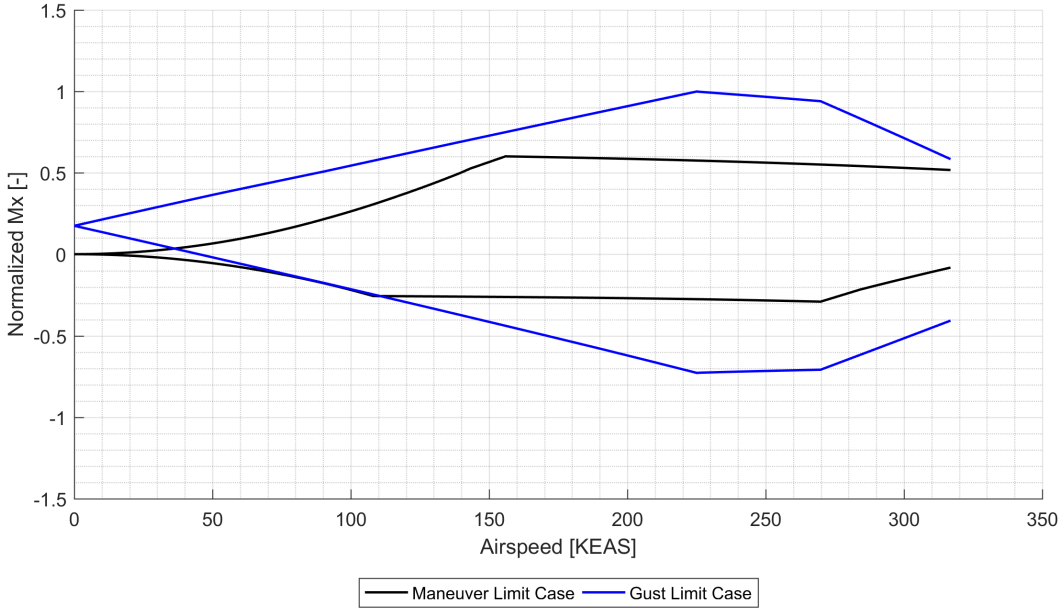

Figure 5.4: Operational V-Mx envelope for inboard wing for the Nastran predicted envelope.

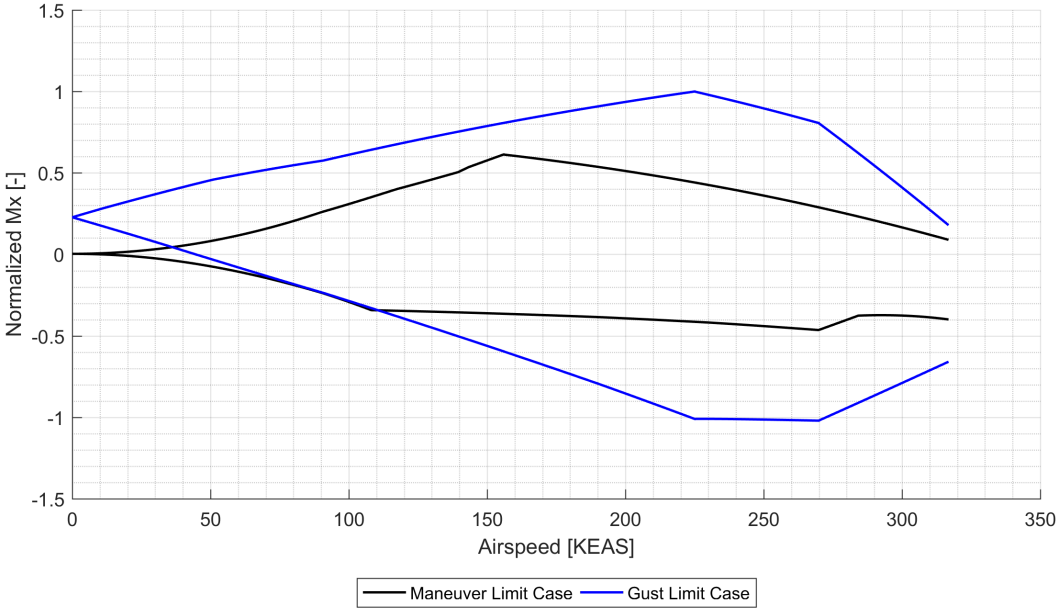

Figure 5.5: Operational V-Mx envelope for outboard wing for the Nastran predicted envelope.

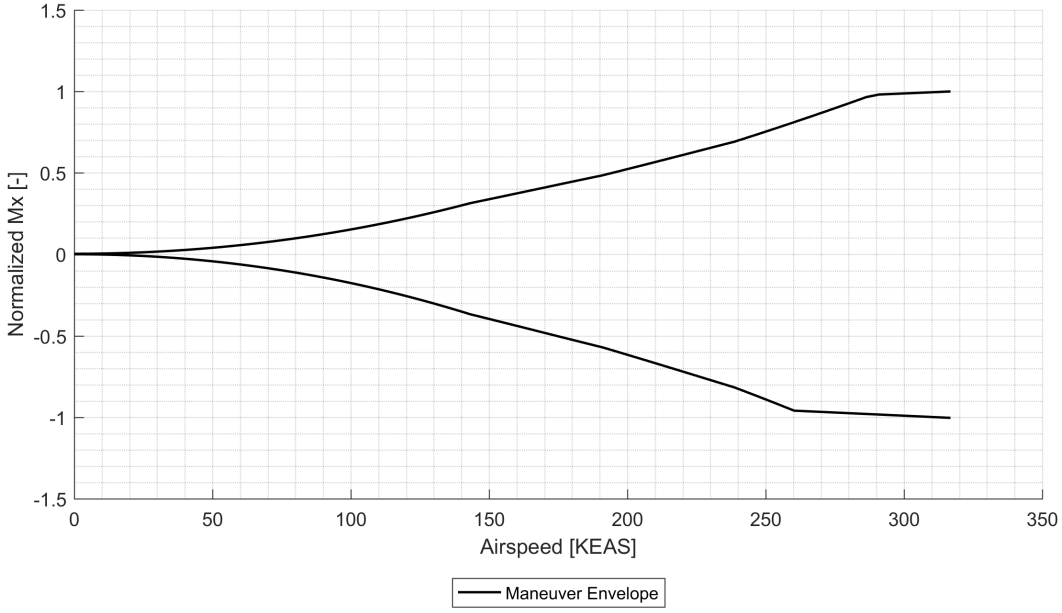

Figure 5.6: Operational V-Mx envelope for winglet showing the Nastran predicted envelope.

Finally, curves of normalized spanwise loads at the critical gust and maneuver cases are also provided. These plots provide another way to interpret the results and better understand the capabilities of the Nastran model. An example showing only the Nastran model predictions along the span for the critical gust and maneuver cases is provided in Fig. 5.7.

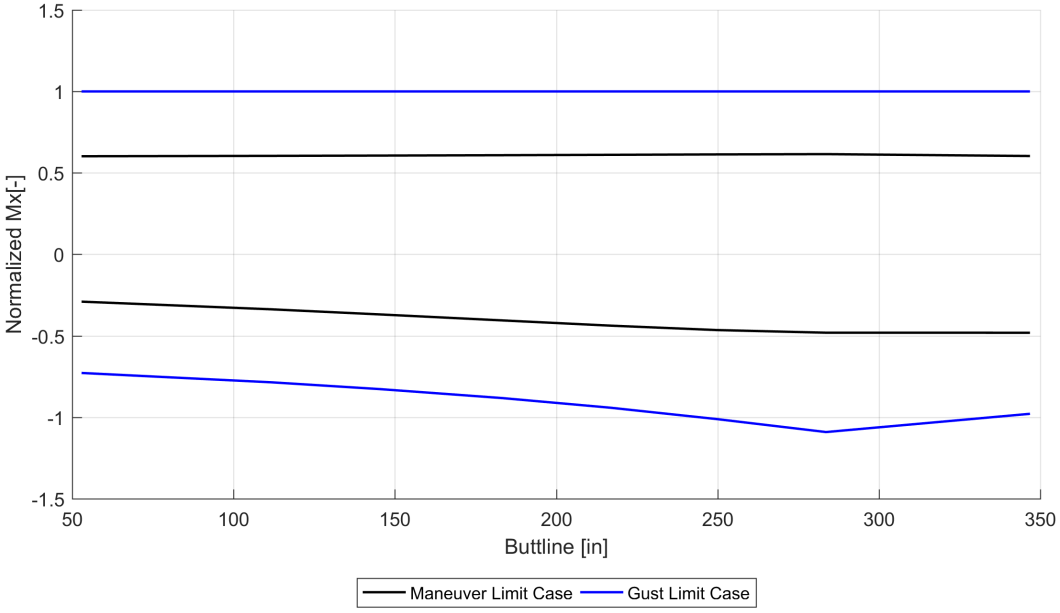

Figure 5.7: Nastran prediction intervals along the span of the wing.

Throughout this section, flight test data and Nastran model predictions will be used to describe the validation and uncertainty quantification process. Furthermore, the difference between the flight test data and Nastran model predictions, $\Delta M_{x_{FT-NAS}}$, is found at discrete flight test points and used for comparisons throughout this section. These values are the error in the Nastran model, and will be denoted throughout this document as ΔM_x.

$$\Delta M_x = M_{x_{FT}} - M_{x_{NAS}} \tag{5.1}$$

Subsequent sections use these methods as the foundation for Nastran model validation and uncertainty quantification. These methods are further built upon and described later, and additional plots are provided to give more insights into the complete model validation process.

5.1 Traditional Methods

Traditional methods typically involve validating analytical flight loads to flight test data using a piecewise approach. First, flight test data are analyzed and shown to be repeatable using a variety of methods, usually by calculating confidence bounds and showing that data from multiple flights are repeatable within those bounds. Next, the analytical model is validated within the validation domain, or the portion of the operational envelope that was flight tested (see descriptions of flight test data in Chapter 2). Comparisons are often plotted in the form of M_x vs. Nz plots, or M_x vs. α plots and shown to fall within a predefined percentage bound (e.g., +/- 10%). From here, the robustness of tools developed for conventional aircraft, such as the Nastran Doublet Lattice Method, are often relied upon to extrapolate to higher airspeeds, load factors, Mach numbers, etc. Testing and validating a small portion of the operational envelope is an acceptable approach because linear aerodynamics can be used to extrapolate the loads to the envelope cases with reasonable accuracy. These extrapolations are often made only with respect to the most dominant flight parameter, Nz or α.

For loads analysis on conventional, fixed-wing aircraft this is a good approach, but it falls short in quantifying the effect of secondary variables on the loads and their effect on the uncertainty of the critical loads cases. As a result, large uncertainties can be seen in cases with large magnitude of secondary variables, such as $Mach$, or how simplifications of unmodeled variables, such as aileron deflections, affect the overall model predictions.

Furthermore, critical loads cases rarely occur at speeds higher than the design cruise Speed (V_C), where loads flight testing is easily conducted. At high speeds ($> V_C$), the airplane tends to be stiffness driven for aeroelastic constraints, as opposed to strength driven, and is substantiated using other methods. Aeroelastic substantiation relies on separate validations of the flutter analysis methods, referring more to acceleration and aerodynamic damping on the airplane. Nevertheless, the loads predictions help to build the foundations for the aeroelastic models, and should be as accurate as possible.

The analyses in Chapter 5.2 and Chapter 5.3 present methods to better understand and quantify error and uncertainty at enveloping loads cases. This section provides an example of traditional methods plotted on V-Mx diagrams, which are used to provide a "baseline" for comparisons to other methods presented in subsequent sections.

As mentioned above, an industry accepted approach to flight loads validation is to validate discrete flight test points to within a prescribed percentage bound, which is typically agreed upon by regulatory authorities and the designer at an early stage in the project. Two plots are provided below, one for the inboard wing and one for the outboard wing, each showing how typical correlations are made between the flight test data and the Nastran model.

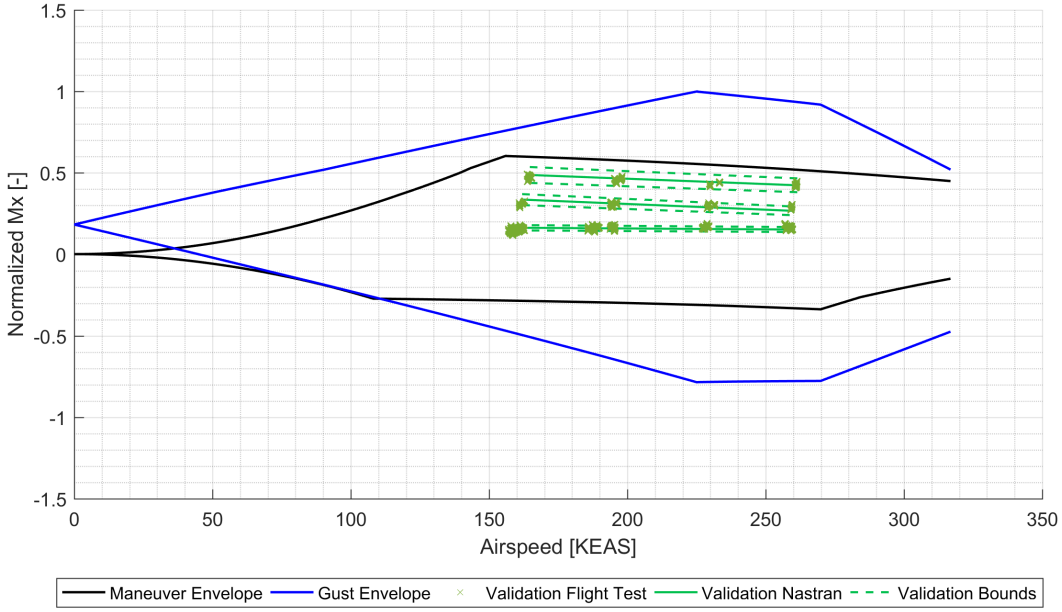

Figure 5.8: Operational V-Mx envelope for inboard wing including traditional validation techniques.

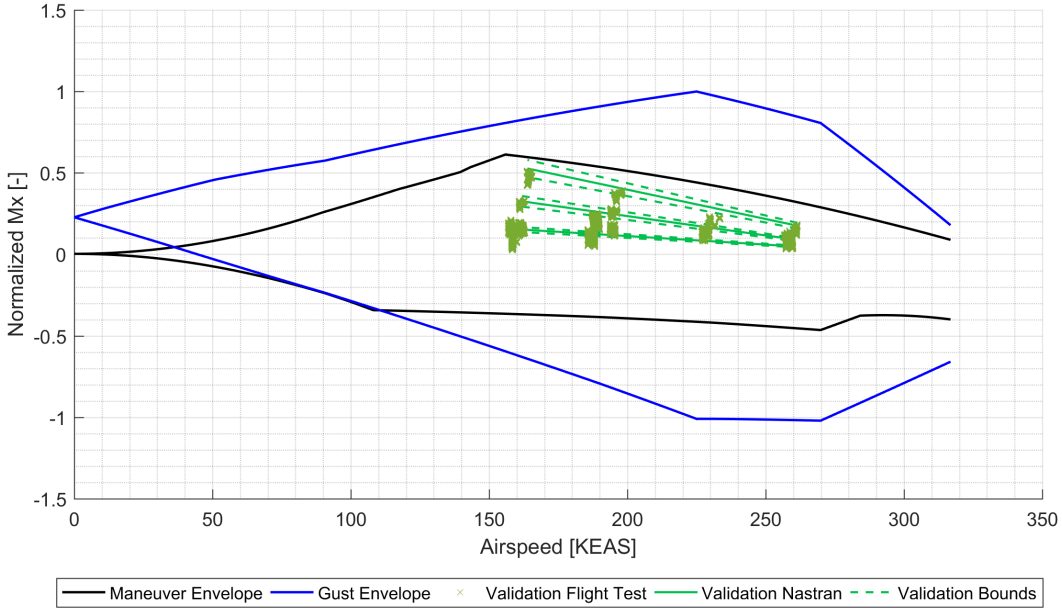

Figure 5.9: Operational V-Mx envelope for outboard wing including traditional validation techniques.

5.2 Nastran Interval Estimate Methods

This section provides a method of computing the uncertainties in the Nastran by comparing the results directly to the flight test data and developing prediction intervals from the mean square error between the two datasets. The prediction intervals were computed on Nastran $M_{x_{NAS}}$ for 95% prediction bounds using the equation shown in Eq. 5.2[20].

$$\hat{y}_i \pm t_{\frac{\alpha}{2},n-(k+1)} \sqrt{\hat{\sigma}^2(1 + x_i(X^T X)^{-1} x_i^T} \tag{5.2}$$

The one-sided student t-value was found for the sample sizes described in Chapter 2. The equation is typically used for linear regression models, but was modified be a function of the mean square error between the Nastran model and flight testing. While Nastran uses a 5-D interpolation, the predictor variables were selected to be of the correct order as the doublet lattice theory implemented in Nastran [14][12] and were used to develop an equivalent prediction interval for the Nastran model. The resulting predictor array of predictor variables, x_i, had 8 terms for each point: M, M^2, q, Nz, δ_{TACS}, δ^2_{TACS}, δ^3_{TACS}, and β.

Using this methodology, the errors in the bending moments are computed and plotted against each of the independent variables. Figures in the subsequent section show the estimated model form uncertainties for the wing Nastran M_x with respect to M, q, Nz, and δ_{TACS}. β is excluded from wing figures because the horizontal portion of the wing is not very sensitive to the sideslip angle. The estimated model form uncertainties of the winglet M_x are examined separately with respect to β and q, the independent variables with the most significant contributions to winglet bending moments.

5.2.1 Nastran Model Uncertainty Quantification

In this section, the estimated model form uncertainties of the Nastran model are plotted in terms of prediction intervals. The prediction intervals show the interval for where 95% of the model predictions will fall. Prediction intervals are presented in the figures as two-dimensional slices of a six-dimensional space. In other words, for each subplot shown the independent variable on the x-axis is allowed to vary while the other four independent variables are held constant, which results in the Nastran M_x plotted on the y-axis. The flight test data shown in each figure are points selected to be within a given tolerance of the slice values. The prediction intervals are computed across the entire range of of the Model 525B operational envelope to show the relative comparison of the validation envelope versus the application envelope.

Fig. 5.22 and Fig. 5.23 provide the estimated model form uncertainty for a section of the inboard wing. The values for the independent variables held constant are $M = 0.55$, $q = 1.60$ lbf/in^2, $Nz = 2.0$ g, $\delta_{TACS} = -20$ deg, and $\beta = 0$ deg. Flight test data points shown are bounded by $0.50 \leq M \leq 0.60$, $1.55 \leq q \leq 1.65$ lbf/in^2, $1.95 \leq Nz \leq 2.05$ g, $-20.5 \leq \delta_{TACS} \leq -19.5$ deg, and $-1.0 \leq \beta \leq 1.0$ deg.

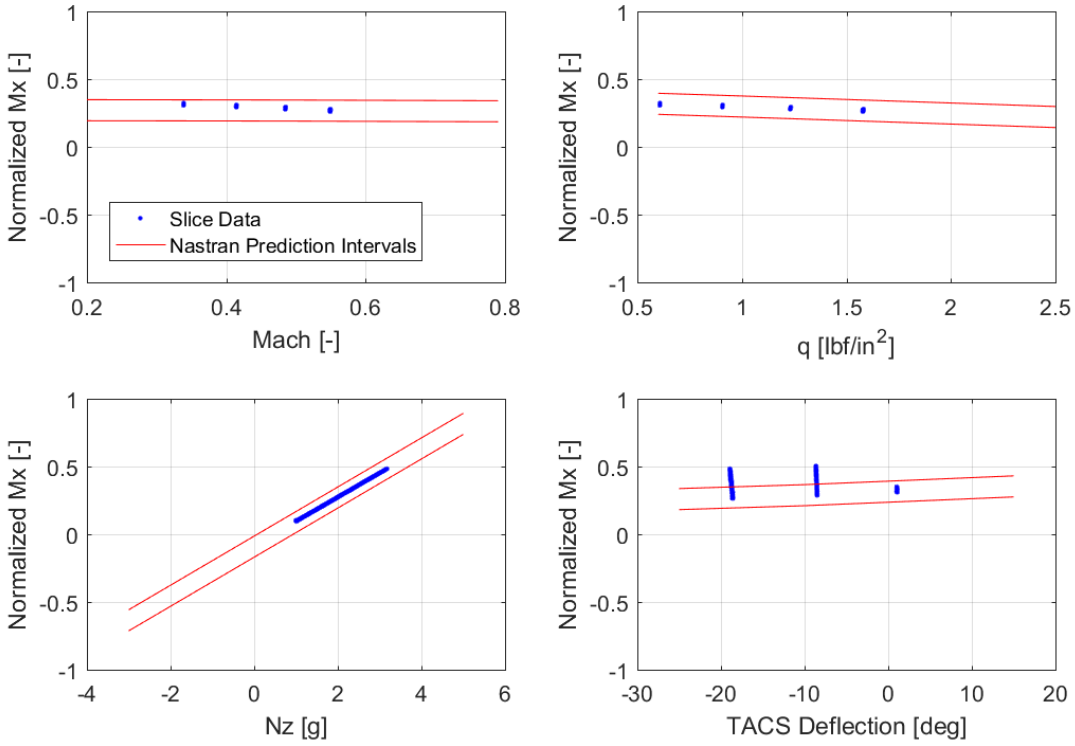

Figure 5.10: Prediction intervals on Nastran M_x for the inboard wing.

Fig. 5.24 provides the estimated model form uncertainty for the winglet. The values for the independent variables held constant are $M = 0.37$, $q = 0.60$ lbf/in^2, $Nz = 1.0$ g, $\delta_{TACS} = 0$ deg, and $\beta = -8$ deg. Flight test data points shown are bounded by $0.27 \leq M \leq 0.47$, $0.59 \leq q \leq 0.61$ lbf/in^2, $0.8 \leq Nz \leq 1.2$ g, $-1.0 \leq \delta_{TACS} \leq 1.0$ deg, and $-1.0 \leq \beta \leq 1.0$ deg.

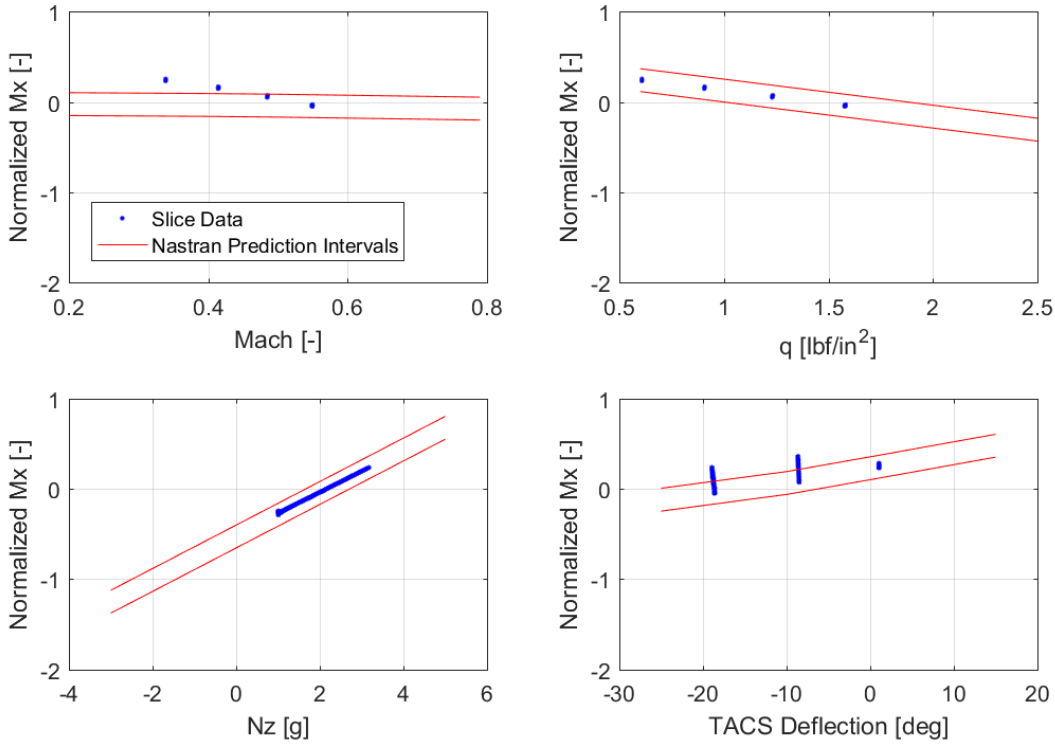

Figure 5.11: Prediction intervals on Nastran M_x for the outboard wing.

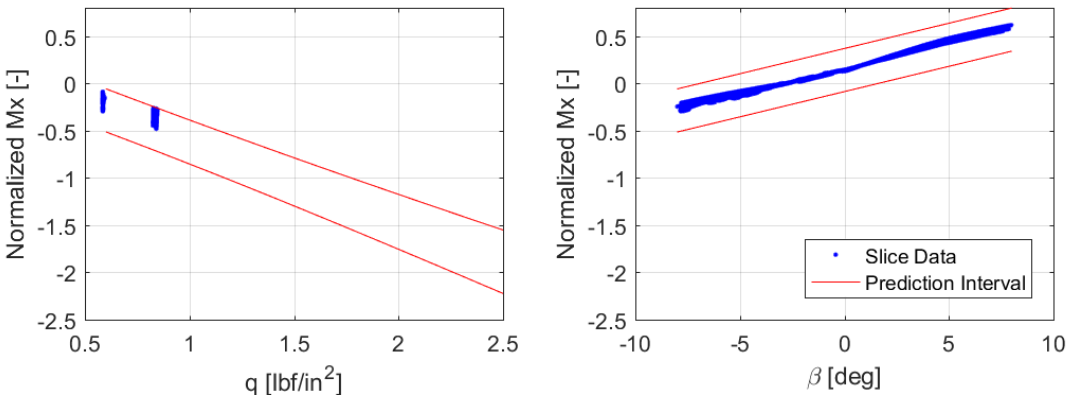

Figure 5.12: Prediction intervals on Nastran M_x for the winglet.

5.2.2 Nastran Model Validation

The validation of the prediction intervals is performed by comparing a new set of flight test data to the original prediction intervals. For a 95% prediction interval, 95% of the dependent variables calculated by the model, in this case bending moments, should fall within the calculated interval. Therefore, validating the model using these methods is a trivial exercise requiring that the prediction intervals be calculated for every data point of a the validation dataset, and it must be shown that 95% of the data points lie within the Nastran prediction intervals.

Comparing the original model prediction intervals in the validation domain to a new set of flight test data shows that the model is accurate and reliable. These validation methods are very similar to those presented in Chapter 5.1, except that the prediction intervals provide a method of predicting error at the edges of the operational envelope using the same mathematical technique as those used to validate the model. Furthermore, it includes the multivariate aspect of the problem in the calculation of the uncertainties.

The Nastran model was easily validated using these methods, with close to 100% of the data points from the validation dataset falling within the Nastran prediction intervals.

5.2.3 Uncertainties in Airplane Operational Envelope

A V-Mx diagram for the inboard wing is shown in the following image.

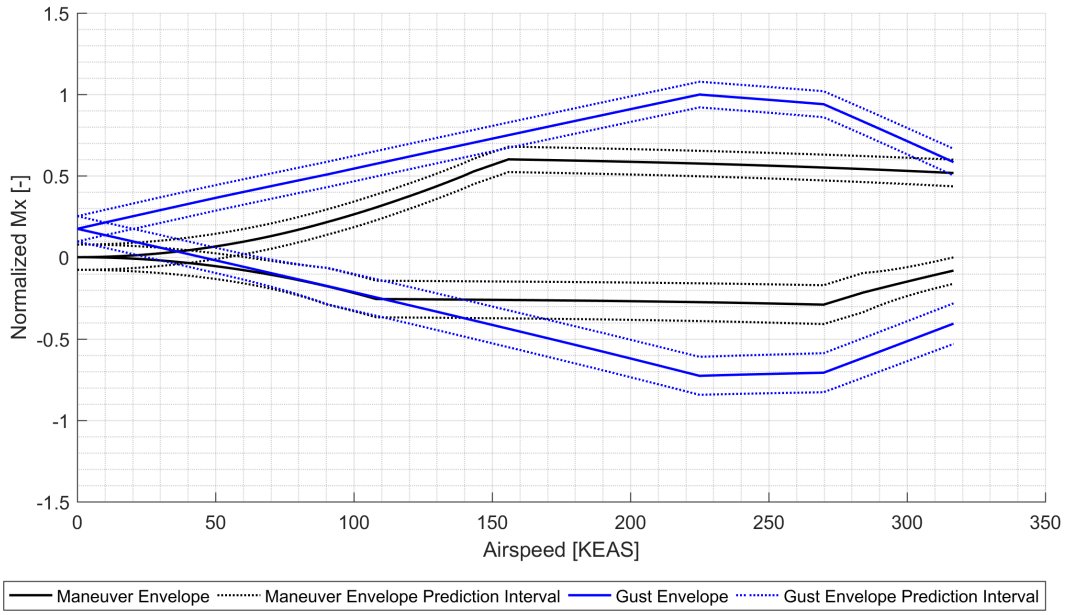

Figure 5.13: Operational V-Mx envelope for inboard wing showing Nastran prediction intervals.

A V-Mx diagram for the outboard wing is shown in the following image.

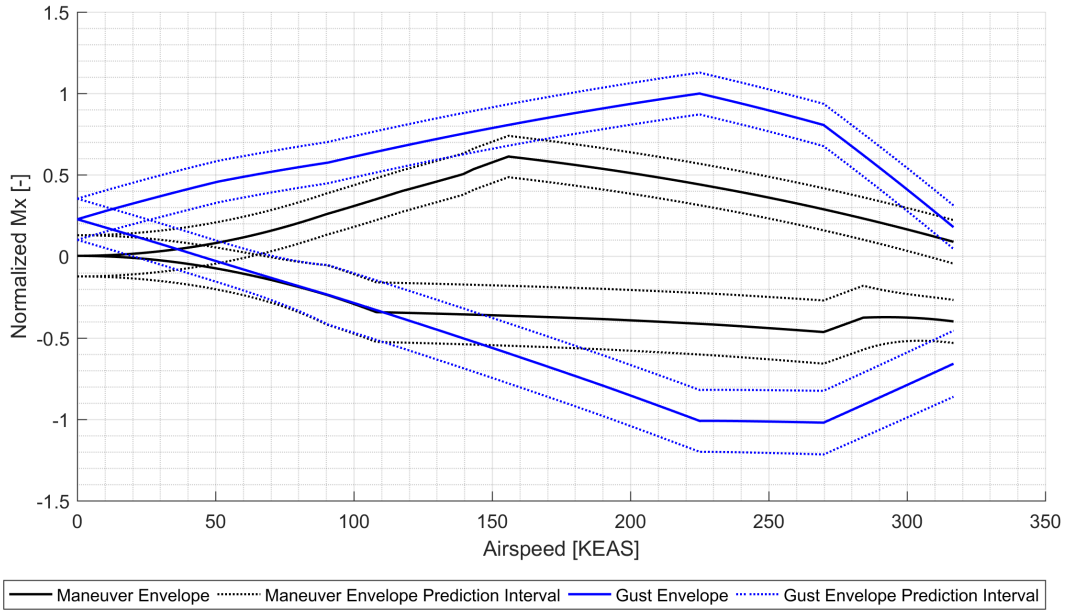

Figure 5.14: Operational V-Mx envelope for outboard wing showing Nastran prediction intervals.

A V-Mx diagram for the winglet is shown in the following image.

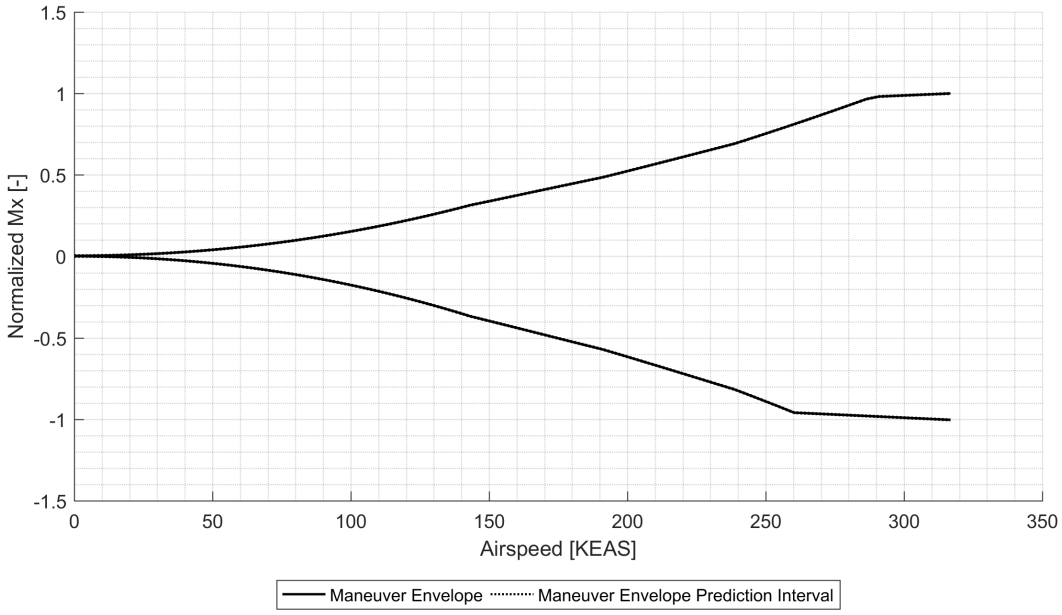

Figure 5.15: Operational V-Mx envelope for winglet showing Nastran prediction intervals.

A plot of the estimated model form uncertainties along the span of the wing for the limit load gust and maneuver cases is shown in the following image.

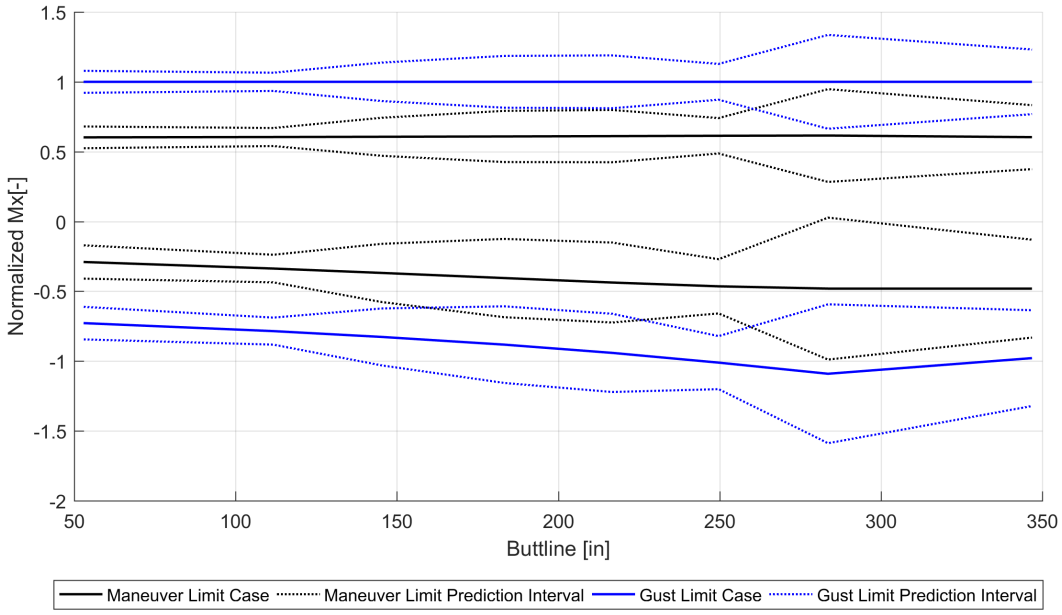

Figure 5.16: Nastran prediction intervals along the span of the wing.

5.3 Multiple Linear Regression Error Modeling

Quantification of the uncertainty is achieved by using a Multiple Linear Regression model (MLR) of the error term between the Nastran and flight test loads. First, the model form of the flight test data is developed in this section to be the minimum order to effectively model the flight test data. Using this model form, a MLR of the error between the Nastran and flight test data is developed, allowing for an accurate prediction of the error term between the two datasets. This error term effectively allows for a validated uncertainty of the Nastran model bending moments to be computed alongside any flight condition for which the model

is used to predict the loads.

Using this methodology, the errors in the bending moments are computed and plotted against each of the independent variables. Similar to the methodology shown in Section 5.2, this section shows estimated model form uncertainty for the wing ΔM_x with respect to M, q, Nz, and δ_{TACS}, and estimated model form uncertainty of the winglet ΔM_x with respect to β and q, the independent variables with the most significant contributions to winglet bending moments.

A nuance of this methodology is that the error term is not necessarily zero mean due to the limitations of the Nastran model tuning. For static loads, the error term predicted by the MLR can be used as an extension of the Nastran model in post-processing to correct the loads for even higher fidelity predictions, which would make static loads error term zero mean. Either way, the estimated uncertainties in the methodology are predicted by the width of the prediction intervals, and can be validated by using additional datasets and by showing that the required percentage of additional flight test data falls within the prediction intervals for the desired confidence level. For other Nastran solutions (see Chapter 3), the error term can be used as an indicator of the error to be expected at a given flight condition, and could be expanded to predict the error on other parameters (such as CL_α itself) that may be more applicable to the other solutions.

5.3.1 Flight Test Multiple Linear Regression Model

The flight test data are also fit with a multiple linear regression (MLR) model to find a regression model form that can effectively characterize the data. The data are fit for aerodynamic bending moment on the wing about the aircraft x-axis (longitudinal axis), M_x. This flight test MLR is not used for tuning or validation, but is instead used to characterize the model form of the flight test data. This same MLR composition is used in Chapter 5 to quantify uncertainty in the Nastran model by developing prediction intervals on the difference between flight test loads and Nastran loads (ΔM_x). In an alternative approach, this MLR could be used to characterize the flight test load for any combination of the predictor variables, and could be validated on its own using procedures similar to those presented in Chapter 5. However, as is described in Chapter 3, tuning of the Nastran model is desired for higher fidelity loads results and for use in other Nastran solutions.

The predictor variables (Nz, M, q, δ_{TACS}, and β) of the model were determined based on the first principles of the trimmed flight condition, but the need for iteration of the terms in the MLR was necessary to find the best fit with the minimum number of terms. The final model form contains 13 terms for the 5 predictor variables, and is shown below. Note that the coefficients of the MLR here are denoted as 'B_i' instead of the customary 'β ' to remove ambiguity.

$$M_{x_{FT}} = B_0 + B_1 Nz + B_2 qM + B_3 qNzM + B_4 q\beta M + B_5 q\delta_{TACS} M + B_6 q\delta_{TACS}^2 M + B_7 q\delta_{TACS}^3 M$$
$$+B_8 qNzM^2 + B_9 q\beta M^2 + B_{10} q\delta_{TACS} M^2 + B_{11} q\delta_{TACS}^2 M^2 + B_{12} q\delta_{TACS}^3 M^2 \tag{5.3}$$

The quality of fit was assessed using basic regression parameters, which were readily available and straightforward. All fits were developed to have high coefficients of correlation and model variables were selected to have low standard errors and p-values [20]. Standard errors were highest in higher-order terms, especially M^2 and δ^3_{TACS} terms, which can be seen consistently throughout the plots presented in this document. For the Mach terms, this higher error is likely due to testing only in low Mach regimes where the Mach terms are mostly linear with respect to dynamic pressure, q, making the mach terms mostly redundant. This error was deemed acceptable because Mach uncertainties are important to consider for an aircraft capable of flying in transonic regimes. For the TACS deflection terms, the error is due to a cubic response of the TACS deflection data that is not much higher in magnitude than the noise of the data itself, causing larger errors than other terms. These errors are recognized and deemed acceptable because they follow the physical response of the system and will help to capture uncertainties in the real-world flight test environment.

Fig. 5.17, Fig. 5.18, and Fig. 5.19 show the frequency distribution and normal probabilities of the residuals for the inboard wing, outboard wing, and winglet, respectively.

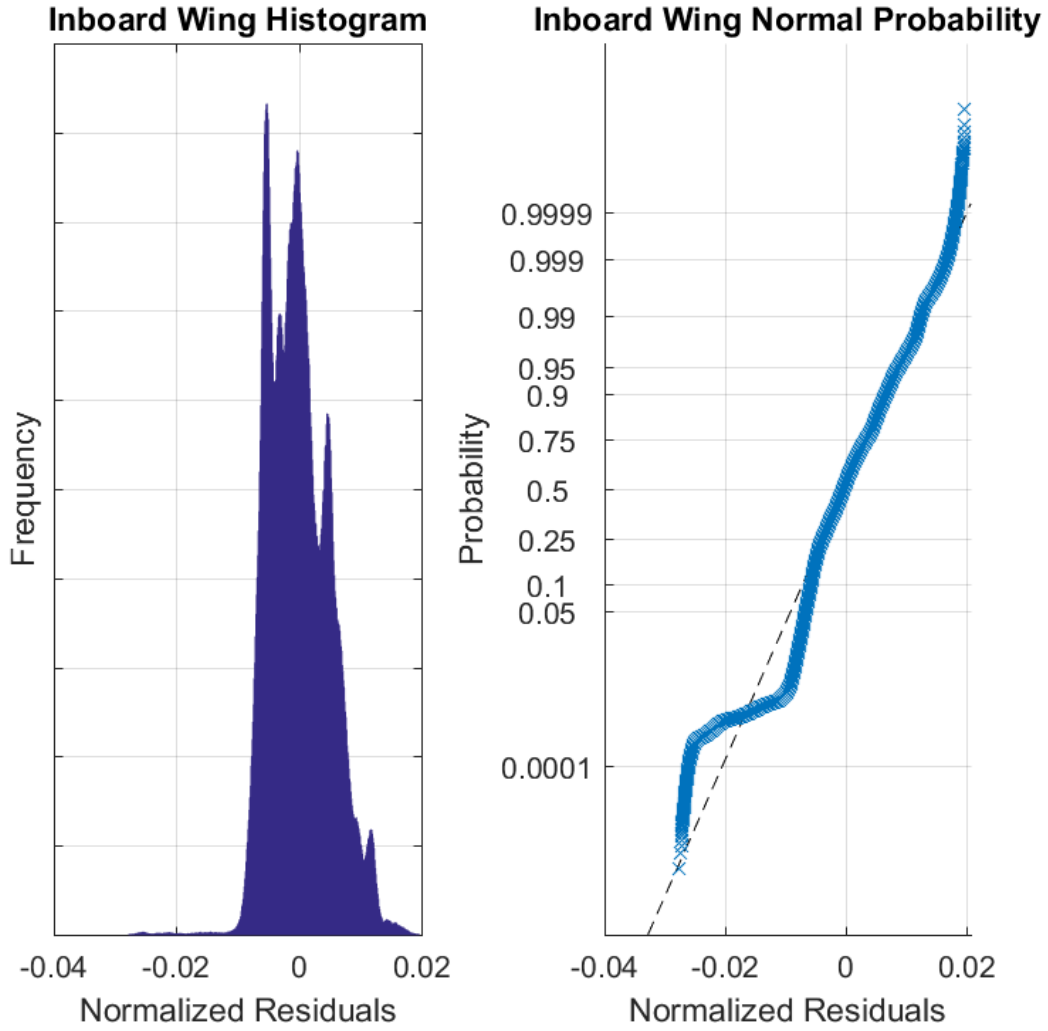

Figure 5.17: Frequency and normal probability of inboard wing residuals

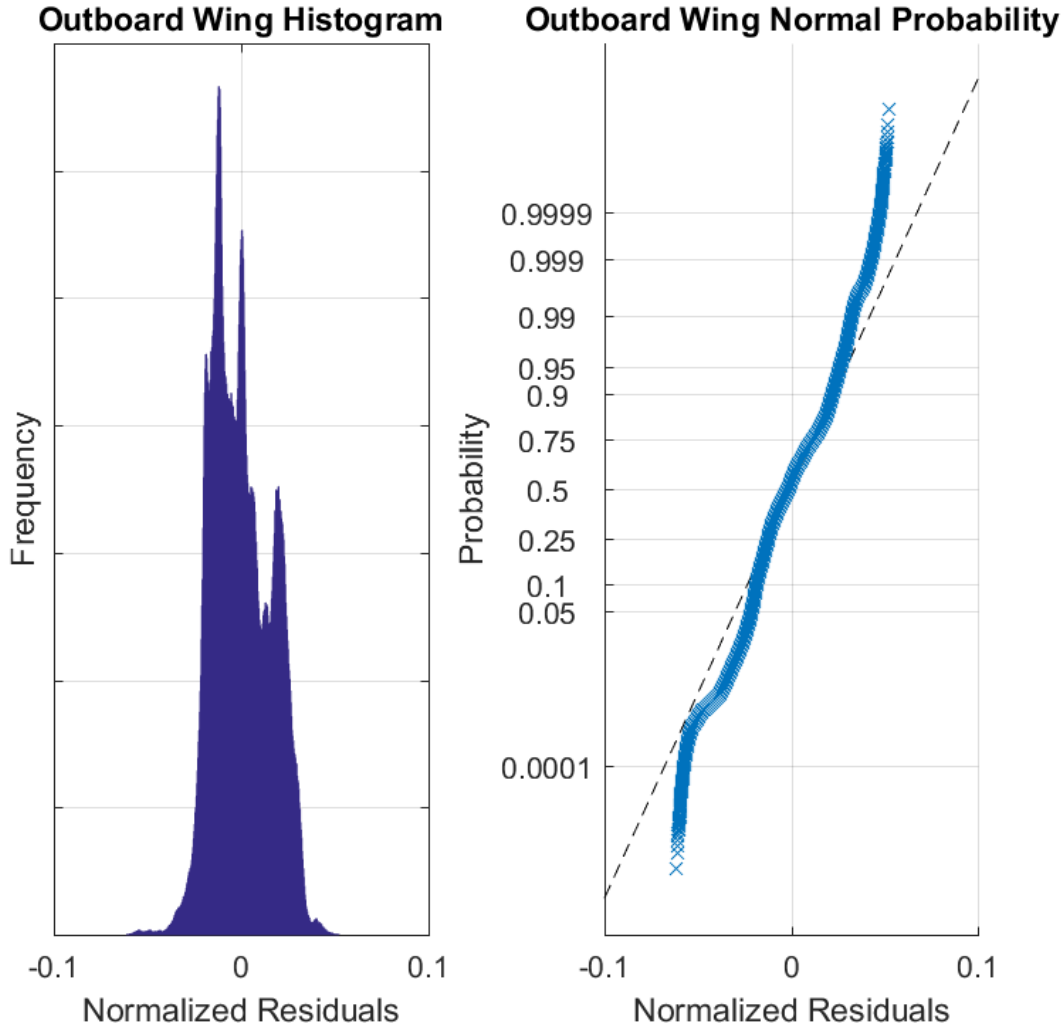

Figure 5.18: Frequency and normal probability of outboard wing residuals

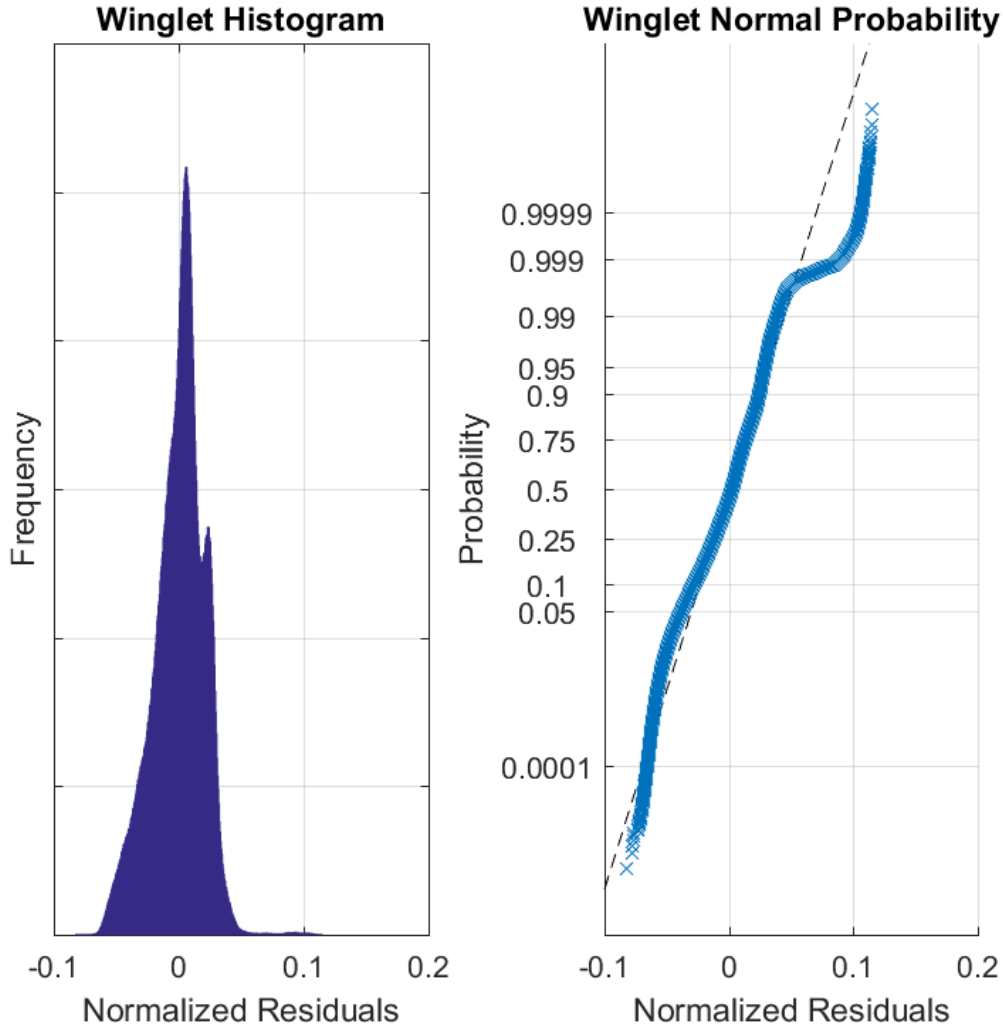

Figure 5.19: Frequency and normal probability of winglet residuals

Some of the most substantial residuals in the plots above can be traced back to sideslip maneuvers. These errors were identified using leverage and Cook's distance plots, which were also used to help the development of the MLR. These plots were used to help identify variables that had a considerable amount of influence on the fit of the MLR [21]. The large

spikes in residuals on the left hand side of the histograms in Fig. 5.17 and Fig. 5.18 are traced back to sideslip maneuvers, which have significantly more leverage on the horizontal portion of the wing than they should (per first principles and the reliable response of the doublet lattice method for this phenomenon). This is most likely due to transients experienced during the sideslip maneuvers, which are ultimately dynamic maneuvers in a real-world flight test environment, especially when the pilot is balancing roll moments in the yaw maneuver with aileron (see Chapter 2.2). A test was performed by developing an MLR without the sideslip maneuvers, and the fit for each location on the wing improved considerably. In the end, however, the sideslip maneuver were deemed necessary to improve the fit of the winglet, as these were by far the most influential maneuvers on winglet bending moments. The leverage and Cook's distance plots for the resulting MLRs are provided below. The sideslip maneuvers are represented by the largest spikes in roughly the center of the Cook's distance plots for all locations on the wing.

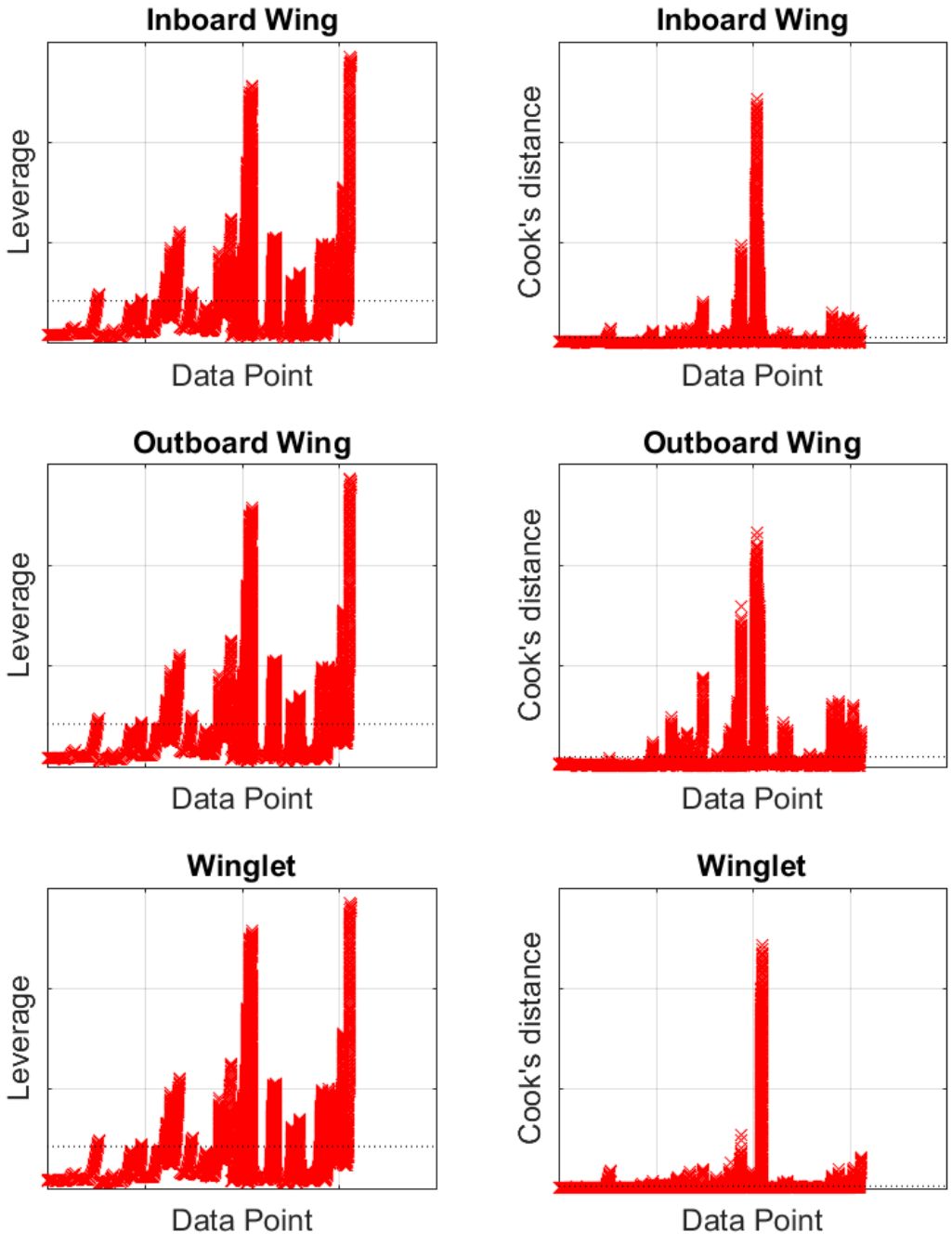

Figure 5.20: Frequency and normal probability of winglet wing residuals

The MLR correlation is shown graphically for the wind-up turns in Fig. 5.21.

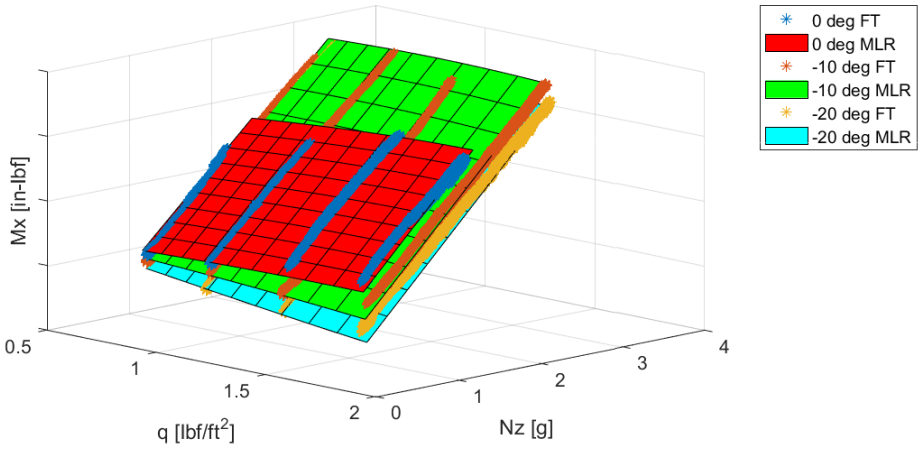

Figure 5.21: Visualization of Flight Test MLR at δ_{TACS} = 0, -10, and -20 deg.

Chapter 5 uses this model form to quantify and validate the uncertainty between the flight test loads and the Nastran model.

An MLR of the error is developed next. The MLR model form is the same as the original developed for the entire flight test dataset. Using the same model form ensures that the error terms are predicted to the same and correct order as the original flight test data, which ensures that predictions beyond the validation envelope are accurately captured. As before, the final model form contains 13 terms for the 5 predictor variables (Nz, M, q, δ_{TACS}, and β), and is shown below.

$$\begin{aligned}\Delta M_{x_{FT-NAS}} = M_{x_{error}} = B_0 + B_1 Nz + B_2 qM + B_3 qNzM + B_4 q\beta M + B_5 q\delta_{TACS} M \\ + B_6 q\delta_{TACS}^2 M + B_7 q\delta_{TACS}^3 M + B_8 qNzM^2 + B_9 q\beta M^2 + B_{10} q\delta_{TACS} M^2 \\ + B_{11} q\delta_{TACS}^2 M^2 + B_{12} q\delta_{TACS}^3 M^2\end{aligned} \tag{5.4}$$

With a validated MLR, the error of the Nastran model can now be quantified at any flight condition. The error on the Nastran model is calculated using the equation shown below.

$$M_x = M_{x_{NAS}} + M_{x_{error}} \tag{5.5}$$

Alternatively, substituting the validated MLR results for the $M_{x_{error}}$ gives us the final M_x with a validated error.

$$M_x = M_{x_{NAS}} + \Delta M_{x_{FT-NAS}} \tag{5.6}$$

This result can be applied at any flight condition, or it can be computed for bounds of the operational envelope to give an accuracy of the model as a whole. For example, the standard V-n Diagram presented in Fig. 2.1 can be customized for a new application to give the accuracy of the model for the gust and maneuver envelopes.

5.3.2 ΔM_x Multiple Linear Regression Uncertainty Quantification

In this section, the uncertainties of the MLR model are quantified. The methods are similar to those presented in Chapter 5.2.1, but the bands of uncertainty are much smaller than the previous methods because the error terms are no longer included as an uncertainty. The MLR technique of error prediction and uncertainty quantification is much more descriptive than the other methods, but it comes with the assumption that the Nastran model is robust and reliable, and thus does not validate the model further than was performed in Chapter 5.2.2. Instead, as described in Chapter 5, this method adds another, dependent model into the mix to describe the relationship between Nastran and flight test data, and validates this new model.

To present the estimated uncertainties, figures similar to those in Chapter 5.2.1 are provided. However, note the large reduction in the size of the interval and the change in mean values of the intervals as these are uncertainties of the Nastran model error, ΔM_x. Each of these figures are selected two-dimensional slices of a six-dimensional space. In other words, for each subplot shown the independent variable on the x-axis is allowed to vary while the other four independent variables are held constant, which results in the ΔM_x response plotted on the y-axis. The flight test data shown in each figure are points selected to be within a given tolerance of the slice values. The prediction intervals are computed across the entire range of of the Model 525B operational envelope to show the relative comparison of the validation envelope versus the application envelope.

Fig. 5.22 and Fig. 5.23 provide the estimated model form uncertainty for a section of the inboard wing. The values for the independent variables held constant are $M = 0.55$, $q = 1.60$ lbf/in^2, $Nz = 2.0$ g, $\delta_{TACS} = -20$ deg, and $\beta = 0$ deg. Flight test data points shown are bounded by $0.50 \leq M \leq 0.60$, $1.55 \leq q \leq 1.65$ lbf/in^2, $1.95 \leq Nz \leq 2.05$ g, $-20.5 \leq \delta_{TACS} \leq -19.5$ deg, and $-1.0 \leq \beta \leq 1.0$ deg.

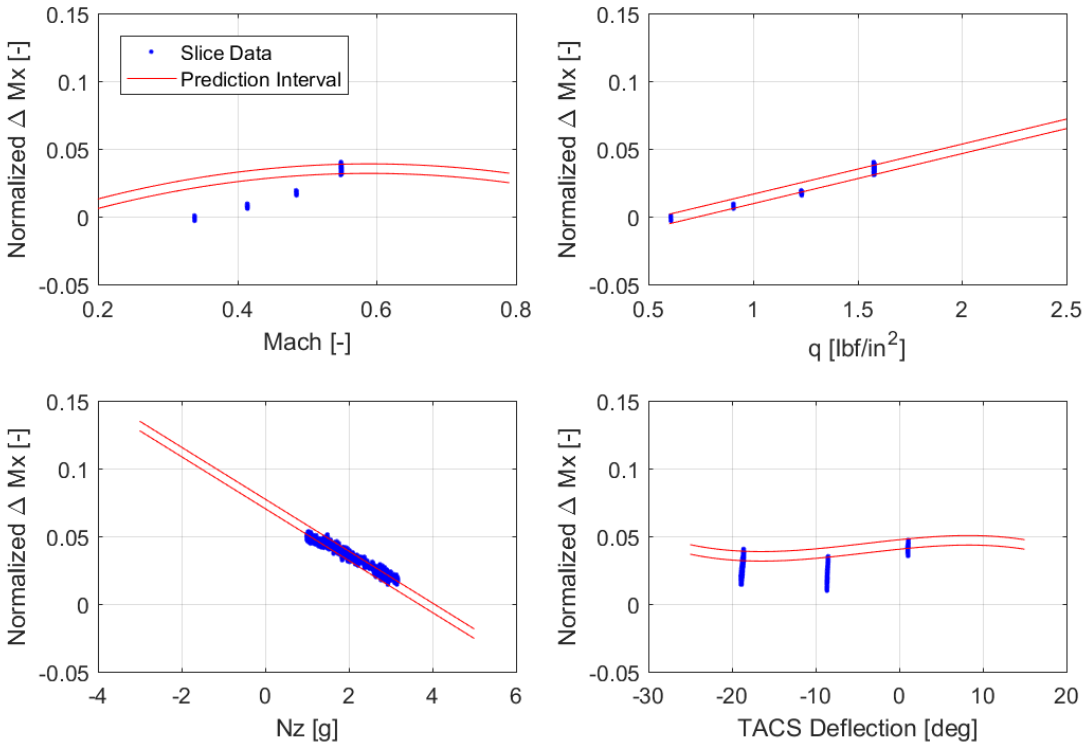

Figure 5.22: Prediction intervals on ΔM_x for the inboard wing.

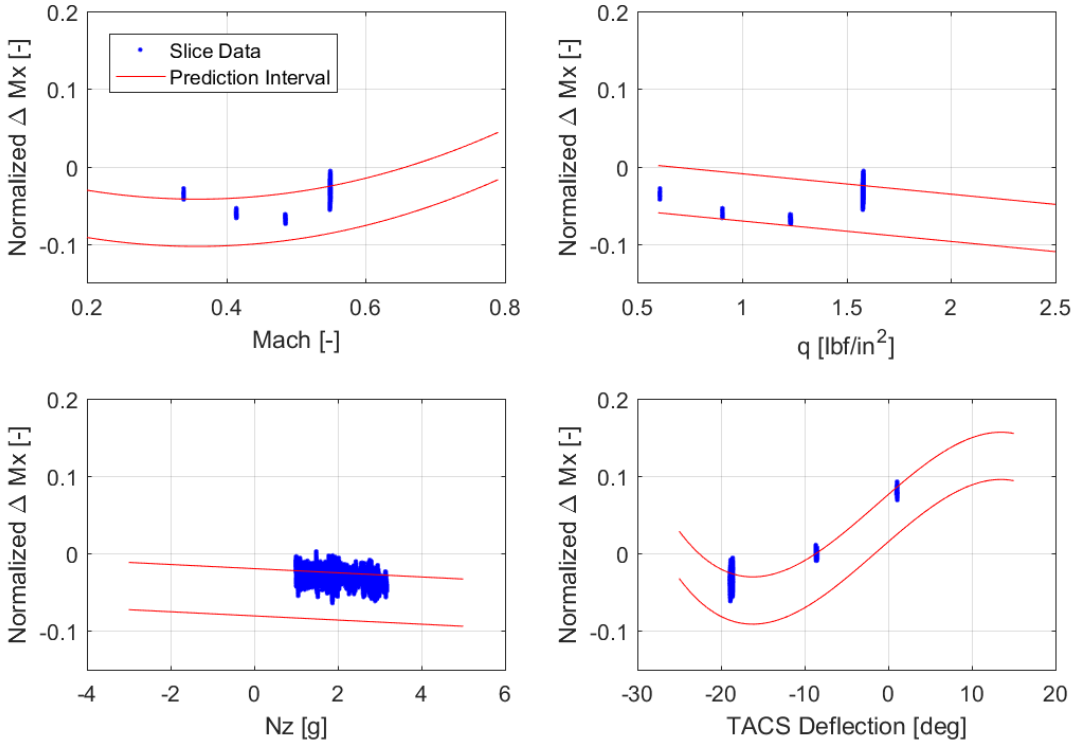

Figure 5.23: Prediction intervals on ΔM_x for the outboard wing.

Fig. 5.24 provides the estimated model form uncertainty for the winglet. The values for the independent variables held constant are $M = 0.37$, $q = 0.60$ lbf/in^2, $Nz = 1.0$ g, $\delta_{TACS} = 0$ deg, and $\beta = -8$ deg. Flight test data points shown are bounded by $0.27 \leq M \leq 0.47$, $0.59 \leq q \leq 0.61$ lbf/in^2, $0.8 \leq Nz \leq 1.2$ g, $-1.0 \leq \delta_{TACS} \leq 1.0$ deg, and $-1.0 \leq \beta \leq 1.0$ deg.

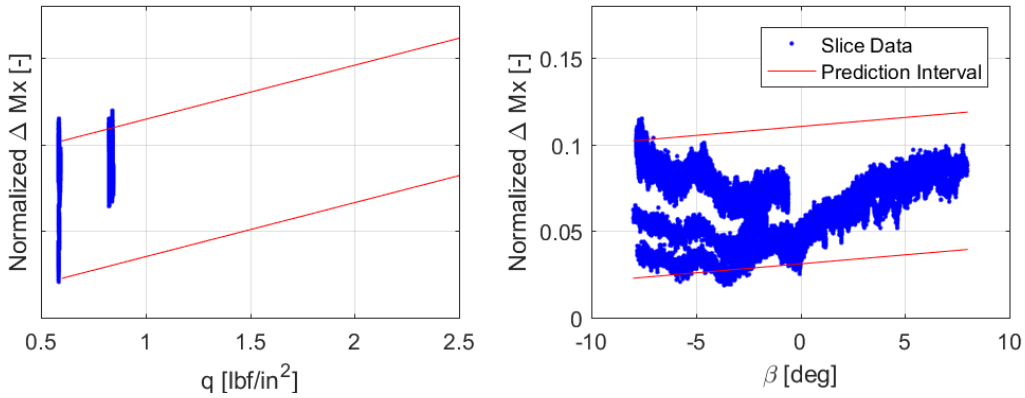

Figure 5.24: Prediction intervals on ΔM_x for the winglet.

5.3.3 ΔM_x Multiple Linear Regression Validation

In this section, methods for validating the MLR model of $\Delta M_{x_{FT-NAS}}$ shown in Eq. 5.4 are described. The MLR model is validated using nearly identical methods to those of the Nastran interval methods described in Chapter 5.2.2. Prediction intervals are validated using a new dataset that was not used for the tuning or prediction interval development. If the results are repeatable, 95% of the predictions will lie within the computed prediction intervals [9]. 95% bounds are selected for this study as this value is most customary, but other bounds may be selected as necessary.

Validating the MLR of $\Delta M_{x_{FT-NAS}}$ proved to be more difficult than validating the lone Nastran model to flight test data (Chapter 5.2.2) or validating the MLR based on $M_{x_{FT}}$ alone. The data used in this study proved to be insufficient, with around 25% of the $\Delta M_{x_{FT-NAS}}$ test points to be within the prediction intervals, which is significantly less than the 95% required to validate the model. The added accuracy of the model made the model more sensitive to error in the measured data. This difficulty indicates that the original assumptions of this method should be revisited, additional modeling fidelity should be included, or additional data should be taken. The validation data set differed slightly in aircraft weight and center of gravity configurations, as well as system operation during the flight test maneuvers. While these differences are minor, they are not negligible for this validation technique. The solution to the problem is to either add the validation datasets to the model development datasets and take more validation data, thereby increasing the error and making the model more robust, or adjust the assumptions of the model to incorporate more variables.

5.3.4 Error Prediction in Airplane Operational Envelope

Changing the V-n diagram to a V-Mx diagram allows the gust and maneuver loads at a particular wing station to be depicted across the operational loads envelope and the error to easily be overlaid to show the model accuracy. In the following images, the bending moment is normalized to the value of the positive limit load Mx case at each particular wing station. Likewise, the Mx error term is normalized to the same value. A V-Mx diagram for the inboard wing is shown in the following image.

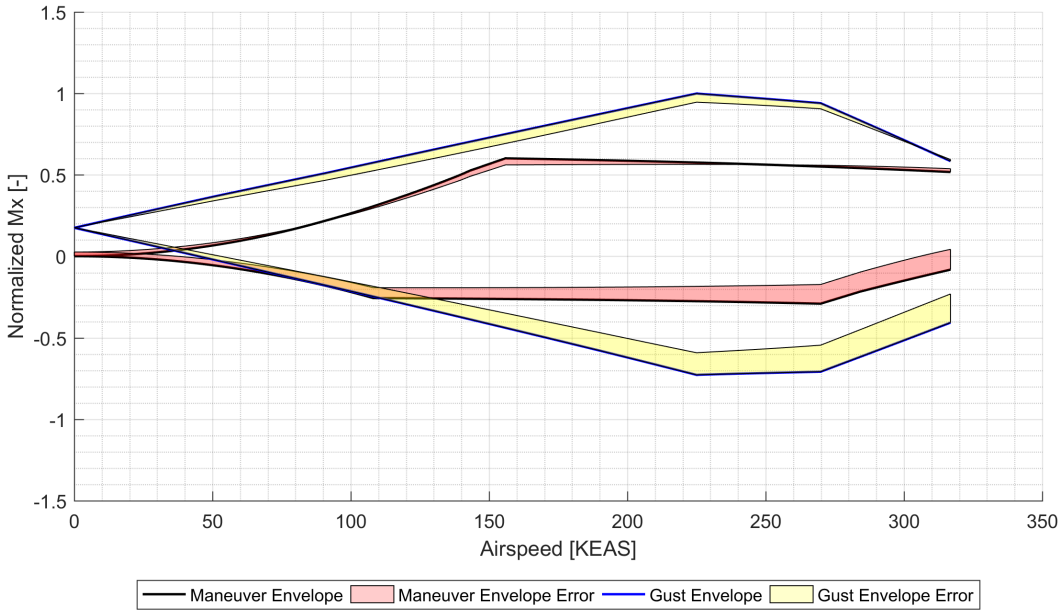

Figure 5.25: MLR predicted error in operational V-Mx envelope for inboard wing.

A V-Mx diagram for the outboard wing is shown in the following image.

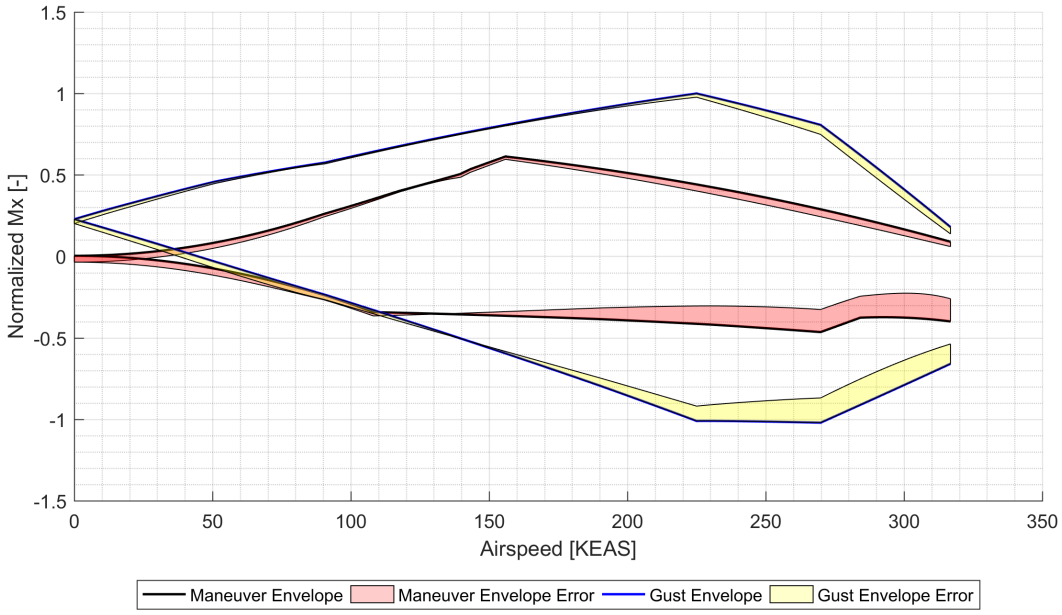

Figure 5.26: MLR predicted error in operational V-Mx envelope for outboard wing.

A V-Mx diagram for the winglet is shown in the following image.

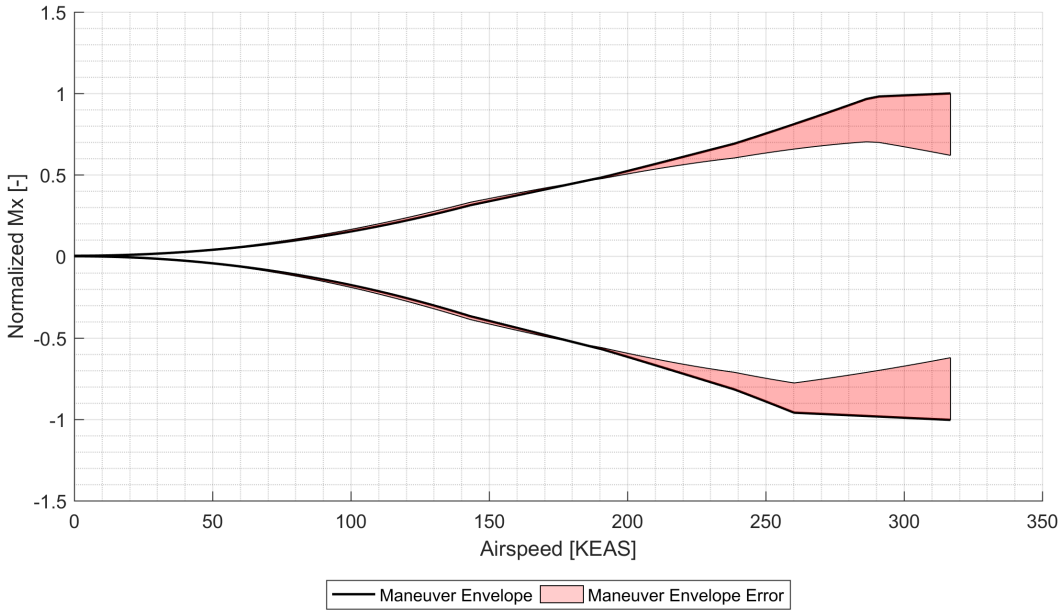

Figure 5.27: MLR predicted error in operational V-Mx envelope for winglet.

A plot of the estimated uncertainties along the span of the wing for the limit load gust and maneuver cases is shown in the following image.

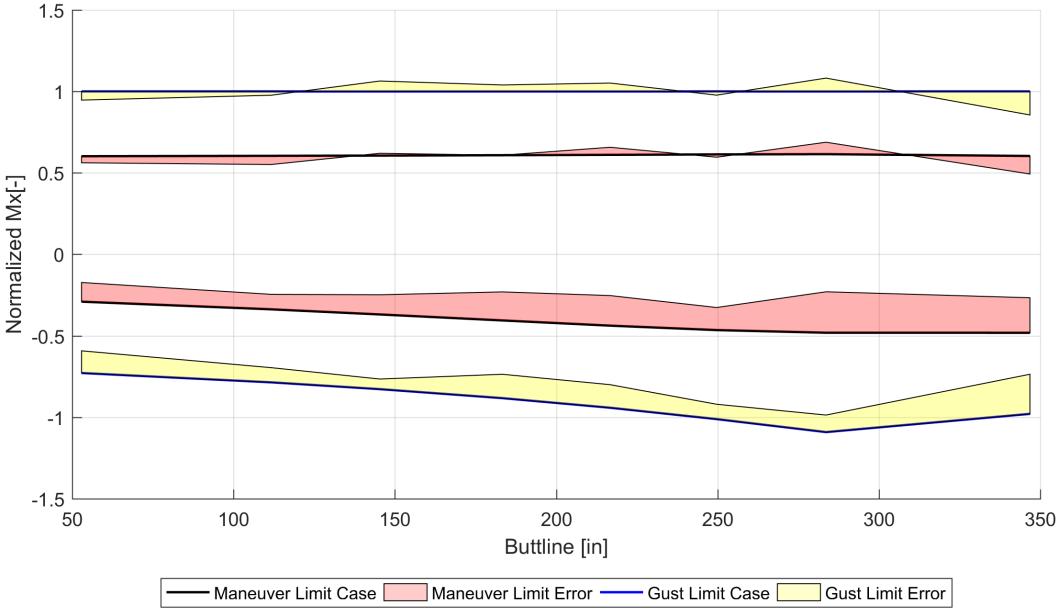

Figure 5.28: MLR predicted error along the span of the wing.

Chapter 6

Conclusion

The framework presented herein describes a method used for tuning and validating flight loads of a Part 23 aircraft. In this study, the framework was applied to a Cessna Model 525B business jet installed with the Tamarack® ATLAS® modification.

The tuning process presented herein provides thorough methods for developing an accurate doublet lattice flight loads model from flight test data. The Model 525B test aircraft was thoroughly instrumented using industry standard methods and a complete flight loads survey was completed. Three types of maneuvers were flown and used for the development and validation of the flight loads model; TACS sweeps, wind-up turns, and sideslip maneuvers. Each of these maneuvers were used to develop and tune the flight loads model as described in Chapter 4 and separate datasets were used for validation and uncertainty quantification purposes. Tuning was carried out using an optimization of the wing spanwise lift distribution

to improve the match between the aerodynamic bending moments derived from flight test and those output from the Nastran model.

The focus of this study was the validation and uncertainty quantification presented in Chapter 5. Two methods were explored for this effort. The first method employed was a very straightforward statistical analysis computing prediction intervals of the Nastran model, which is a function based on the number of sample datasets and the error between the tuned model and the flight test data. The prediction intervals themselves quantify the estimated model form uncertainties and are straightforward to validate.

A second method employed the use of a Multiple Linear Regression (MLR) model to better quantify the error between the Nastran loads model outputs and the flight test loads. This model provided a more accurate description of the error between Nastran and flight test loads, gave more insight into the response of the model, and showed where improvements could be made. Any divergences between the Nastran and flight test loads results are indicators of modeling limitations, where more flight test data, model updating, or erroneous flight test data may be present. Furthermore, this method reduces the uncertainties in the model. While providing these valuable insights, this method also proved to be more problematic to validate as it is more sensitive to sparse data. Therefore, its greatest value may be in a check for the validity and reliability of flight test data, where it can be used for a "quick and dirty" check of reliability and repeatability.

The two methods provide a trade-off between simplicity and improved accuracy and understanding of the model predictive capabilities. The first model is a very straightforward

and simple approach, but will deliver greater uncertainty bounds. The second method was added because of nearly unavoidable, but predictable nonzero mean errors between a computational physics model like the doublet lattice method in practical applications. This method quantifies those errors by adding a secondary model, significantly increasing complexity but adding very valuable insights into the limitations of the doublet lattice methods. The specific application of the validation techniques and the accuracy to which they must be validated should dictate which method to use.

Bibliography

[1] Guida, N. R., "Active Winglet," *US Patent 7,900,877 B1*, March 2011.

[2] "14 CFR Part 23 - Airworthiness Standards: Normal, Utility, Acrobatic, and Commuter Category Airplanes", Amendment No. 23-62, Federal Aviation Administration, 31 Jan. 2012.

[3] Roy, C. J., and Oberkampf, W. L., "A Comprehensive Framework for Verification, Validation, and Uncertainty Quantification in Scientific Computing," *Computer Methods in Applied Mechanics and Engineering*, Vol. 200, 15 June 2011, pp. 2131–2444.

[4] Skopinski, T. H., Aiken, W. S., Jr., and Huston, W. B., *Calibration of Strain-Gage Installations in Aircraft Structures for the Measurement of Flight Loads*, NACA-TR-1178, National Advisory Committee for Aeronautics, Langley Aeronautical Lab, Langley Field, VA, 01 Jan. 1954.

[5] Gonzalez, M., Gogu, C., Binaud, N., Espinosa, C., Morlier, J., and Quoniam, S., "Uncertainty Quantification in Aircraft Load Calibration," *10th World Congress on Structural and Multidisciplinary Optimization*, May 2013.

[6] Tartaruga, I., Cooper, J. E., Sartor, P., and Lowenberg, M., "Efficient Prediction and Uncertainty Propagation of Correlated Loads," *AIAA SciTech Forum Paper 2015-1847*, January 2015.

[7] Cook, R. G., Wales, C. J. A., Gaitonde, A. L., Jones, D. P., and Cooper, J. E., "Uncertainty Quantification in Gust Loads Analysis of A Highly Flexible Aicraft Wing," *International Forum on Aeroelasticity and Structural Dynamics (IFASD 2017)*, June 2017.

[8] Menga, E., Lopez, C., Hernandez, S., Baldomir, A., Romero, I., and Sanchez, M. J., "Uncertainty Quantification in the Dynamic Response of Assembled Structures," *International Forum on Aeroelasticity and Structural Dynamics (IFASD 2017)*, May 2017.

[9] Hale, L. E., Patil, M., and Roy, C. J., "Aerodynamic Parameter Identification and Uncertainty Quantification for Small Unmanned Aircraft," *Journal of Guidance, Control, and Dynamics*, Vol. 40, No. 3, 2017, pp. 680–691. doi:10.2514/1.G000582.

[10] Lomax, T. L., *Structural Loads Analysis for Commercial Transport Aircraft: Theory and Practice*, AIAA Education Series, American Institute of Aeronautics and Astronautics, Inc., Reston, VA, 1996.

[11] Tang, M. H., Sefic, W. J., Sheldon, R. G., *Comparison of Concurrent Strain Gage and Pressure Transducer Measured Flight Load on a Lifting Surface Reentry Vehicle and Correlation with Wind Tunnel Predictions*, NASA Technical Paper 1331, National Aeronautics and Space Administration, Dryden Flight Research Center, 1978.

[12] "NX Nastran 10 Aeroelastic Analysis User's Guide," 2014.

[13] "NX Nastran 10 Quick Reference Guide," 2014.

[14] Blair, M., "A Compilation of the Mathematics Leading to the Doublet Lattice Method," WL-TR-92-3028, Mar 1992.

[15] Giesing, J. P., Kalman, T. P., Rodden, W. P., "Correction Factor Techniques for Improving Aerodynamic Prediction Methods", Douglas Aircraft Corporation, Long Beach, CA, 1976.

[16] Baker, M. L., "CFD Based Corrections for Linear Aerodynamic Methods," Numerical Unsteady Aerodynamic and Aeroelastic Simulation, AGARD 822, March 1998.

[17] Baker, M. L., Goggin, P. J., and Yuan, K. A., "Calculations of Corrections to Linear Aerodynamic Methods for Static and Dynamic analysis and Design", AIAA 98-2072, American Institute of Aeronautics and Astronautics, 1998.

[18] Thormann, R., Dimitrov, D., "Correction of aerodynamic influence matrices for transonic flow", *CEAS Aeronaut J 5:435–446 DOI 10.1007/s13272-014-0114-3*, 2014.

[19] Riley, M. E., "Quantification of Model-Form, Predictive, and Parametric Uncertainties in Simulation-Based Design," *Ph.D. Dissertation*, 2011.

[20] Seber, G. A. F., and Lee, A. J., *Linear Regression Analysis*, Springer-Verlag New York, Inc., New York, NY, 2000.

[21] Atkinson, A. Riani, M., *Robust Diagnostic Regression Analysis*, Wiley Series in Probability and Statistics, John Wiley & Sons, Inc., Hoboken, NJ, 2003.